Shackleton, N.J., Curry, W.B., Richter, C., and Bralower, T.J. (Eds.), 1997
Proceedings of the Ocean Drilling Program, Scientific Results, Vol. 154

6. DEVELOPMENT OF A HIGH-QUALITY NATURAL GAMMA DATA SET FROM THE CEARA RISE: CRITICAL GROUNDWORK FOR CORE AND LOG DATA INTEGRATION[1]

Teresa A. King[2] and William G. Ellis, Jr.[2, 3]

ABSTRACT

Natural gamma-ray emissions are potentially powerful indicators of terrigenous sediment composition. At the Ceara Rise, such data can provide insight to the evolution of terrigenous fluxes from the South American continent during the late Neogene. Although log-derived natural gamma emissions data have relatively lower noise levels than core-derived data, they are limited by a vertical resolution on the order of 0.5–1 m. Conversely, natural gamma-ray emissions data collected from cored sediments during Leg 154, although noisier, have a depth resolution on the order of 10 cm. Thus, the core data provide both a strong complement to downhole measurements of natural gamma as well as higher vertical (depth) resolution. Combining the two measurements provides for reconstruction of variations in terrigenous sedimentation over the past 35 m.y. encompassing both orbital (~0.01–~0.1 m.y.) and tectonic (>0.1 m.y.) time scales. In this paper we present a method to obtain robust discretely sampled, core-derived natural gamma-ray data from multiple holes. A "stacked" data set derived from multiple holes has less noise (lower mean square error) at all natural gamma-ray emissions channels, and thus is superior to core-derived natural gamma data taken from a single APC/XCB hole. A comparison of the stacked core-derived natural gamma data to the log-derived natural gamma data for a 12-m.y.-long Neogene sequence from Site 926 documents the general attenuation of log-derived measurements relative to stacked core-derived measurements for most orbital-scale and tectonic-scale oscillations. This result suggests that high-quality core-derived measurements of natural gamma-ray emissions can, under the correct circumstances, provide superior resolution and reliability to log-derived measurements over a large range of time scales.

INTRODUCTION

Plate tectonic movements during the late Neogene resulted in significant uplift of the northeastern Andes and development of the Amazon drainage system; these tectonic events resulted in the Miocene development of the Amazon River as a transcontinental drainage system into the Atlantic Ocean (Hoorn et al., 1995). The history of this major reorganization of drainage systems is recorded in sediments distal to the Amazon Fan, on the Ceara Rise. Sediments from the Ceara Rise provide an opportunity to reconstruct this history of terrigenous flux and composition (Curry, Shackleton, Richter, et al., 1995; Dobson, et al., this volume; King et al., this volume).

Natural gamma-ray activity in sediments arises from the potassium, uranium, and thorium content of what is typically the terrigenous fraction. Naturally occurring isotopes of these elements (^{40}K, ^{238}U, ^{235}U, and ^{232}Th) produce gamma rays as they decay to stable isotopes of Ar and Pb. The measurable gamma-ray emissions provide an estimate of potassium, uranium, and thorium in the sediment. Results from previous studies using downhole logs (e.g., Fertl, 1979) have demonstrated that the relative concentrations of K and Th obtained from gamma-ray measurements can be used to distinguish clay mineral compositions. At the Ceara Rise, shipboard results demonstrated convincingly that the proportion of K-bearing sediments and Th-bearing sediments, as seen in the log gamma-ray derived Th/K ratio, corresponded with the relative abundance of illite (5%–6% K content) and kaolinite (<1% K content) (Fig. 1; Curry, Shackleton, Richter, et al., 1995). As Figure 1 suggests, natural gamma activity provides a powerful means to estimate past variations in kaolinite and illite concentrations on the Ceara Rise.

Natural gamma emissions data collected on Ocean Drilling Program (ODP) Leg 154 offer a unique opportunity to characterize the compositional changes in terrigenous sediments over the late Neogene at orbital-scale resolution. Core-derived natural gamma-ray emissions measurements were collected at approximately 10-cm spacing through most of the sediments recovered at Sites 926–929. Measurements were typically collected using a 10-s counting time; although greater counting times are in theory desirable, it was a priority of the Leg 154 scientific party to collect natural gamma-ray measurements on as many cores as possible. Because Leg 154 had record-breaking recovery, the counting time for natural gamma placed a restriction on core flow through the shipboard laboratories. Experiments conducted during Leg 154 indicated that 15- or 30-s count times for the APC- and XCB-cored sediments did not appreciably reduce the variance of the natural gamma-ray counts compared to 10-s count times. As a result, the scientific party chose to make 10-s counts so that as much core as possible could be measured. The methods presented here demonstrate how those 10-s measurements can be combined from separate holes (multiple ensembles) to produce a more reliable measurement at each depth.

Downhole logs of natural gamma activity were also obtained at each Leg 154 site. Log-derived natural gamma activity (measured in API units) provide an opportunity to obtain a reliable view of terrigenous composition. However, whereas the intrinsic resolution of the tool is 45 cm, emprical studies have suggested that the practical resolution of the natural gamma tool is greater than 50 cm (Harris et al., 1995; Curry, Shackleton, Richter, et al., 1995). Core-derived natural gamma activity (measured as counts/s), on the other hand provide an opportunity to study changes in terrigenous composition at 10- to 20-cm resolution. These differing resolutions are illustrated in Figure 2, which compares a 50-m portion of the raw, uncorrected core natural gamma activity data from Site 926 to the log natural gamma activity. Note, however, that although the core-derived data has greater sampling resolution, the core-derived data also has much greater scatter.

When converted to time-domain, rather than depth-domain, differences, the implications of this differing resolution become more

[1]Shackleton, N.J., Curry, W.B., Richter, C., and Bralower, T.J. (Eds.), 1997. *Proc. ODP, Sci. Results,* 154: College Station, TX (Ocean Drilling Program).
[2]Graduate School of Oceanography, University of Rhode Island, Narragansett, RI 02882, U.S.A. tking@gsosun1.gso.uri.edu
[3]Present address: Corning School of Ocean Studies, Maine Maritime Academy, Castine, ME 04420, U.S.A.

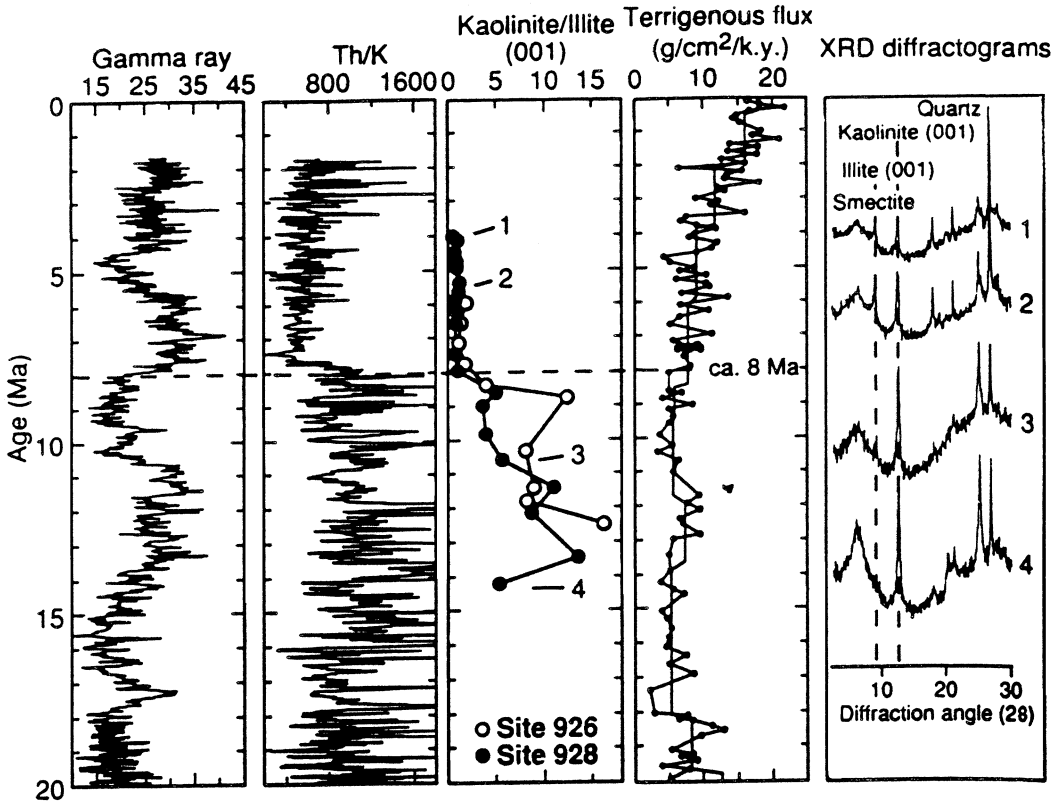

Figure 1. Log natural gamma data from Site 926 are total gamma-ray emissions; Th/K ratios are compared to observed kaolinite/illite ratios, terrigenous mass fluxes, and XRD diffractograms (from Curry, Shackleton, Richter, et al., 1995).

significant. Table 1 gives the average sedimentation rates for the last 5 m.y. at Sites 925–929. Although the core-derived natural gamma-ray data record terrigenous sediment variations on orbital time scales through most of the sedimentary sequence at the Ceara Rise, the log-derived data, having a lower depth resolution, can only capture orbital-scale variability in intervals having very high sedimentation rates. For example, assuming a 45-cm vertical resolution for the natural gamma-ray tool, sedimentation rates must be in excess of 5 cm/k.y. to avoid aliasing of orbital-scale oscillations into lower frequencies (for a full discussion of aliasing, see Pisias and Mix, 1988). On the other hand, core-derived data sampled at 10-cm spacing can theoretically detect orbital scale oscillations without aliasing at average sedimentation rates above 1 cm/k.y. However, by integrating the core and the log data, one has the opportunity to characterize terrigenous sedimentation over multiple time scales, from orbital to tectonic. Thus, despite the addition of some noise to the core-derived natural gamma measurements, the benefit gained from having orbital-resolution measurements is significant.

In this paper, we combine core-derived natural gamma data from multiple APC and XCB holes that have been background-corrected and "cleaned" to produce a single profile of natural gamma activity for those sites having multiple hole natural gamma data (Sites 926, 928, 929; unfortunately because of time constraints, Sites 925 and 927 did not have natural gamma activity collected in each hole). The primary purpose is to gain a single, high-resolution, lower mean-square error core-derived natural gamma-ray depth series for each site. By considering each natural gamma measurement at the same depth in each hole a separate statistical realization of the "true" natural gamma activity at that depth, and by averaging those multiple realizations, one obtains an estimate having, on average, less random error. One also gains, in averaging the multiple hole data, a quantitative estimate of hole-to-hole variability in sedimentation. These estimates are then combined with estimates of log resolution and variability to further assess core and log resolution from ODP holes (deMenocal and King, 1995). We present a method to combine multiple hole data into a single record. We provide decimeter-scale hole-to-hole correlations for Leg 154 sites and the depth transformation from meters composite depth (mcd) to revised meters composite depth (rmcd). Finally, we compare the stacked core-derived natural gamma data with the log-derived natural gamma data for the late Neogene portion of Site 926.

METHODS

Data Reduction

Natural gamma and magnetic susceptibility data were cleaned before the data were correlated at high resolution. By cleaning, we mean that for each core in each hole at each site, outliers were removed, measurements made in disturbed intervals were removed, and measurements made in voids were removed. Core-derived natural gamma-ray data, which are recorded in total counts (Typically, counting times were 10 s during Leg 154), were converted to counts per second; background levels of natural gamma activity (calculated during Leg 154; Curry, Shackleton, Richter, et al., 1995) were removed from each channel. Natural gamma activity data were not converted to American Petroleum Institute (API) units, as described by Hoppie et al. (1994) and Lyle et al. (in press), primarily because the Gamma-Ray Attenuation Porosity Evaluator (GRAPE) densities at several sites were unreliable, owing to multiple problems including drift and calibration (see "Explanatory Notes Addendum" of Curry, Shackleton, Richter, et al., 1995). Because the large errors in the GRAPE data would only add to the noise already present in the core-derived natural gamma, thus degrading the quality of the resulting

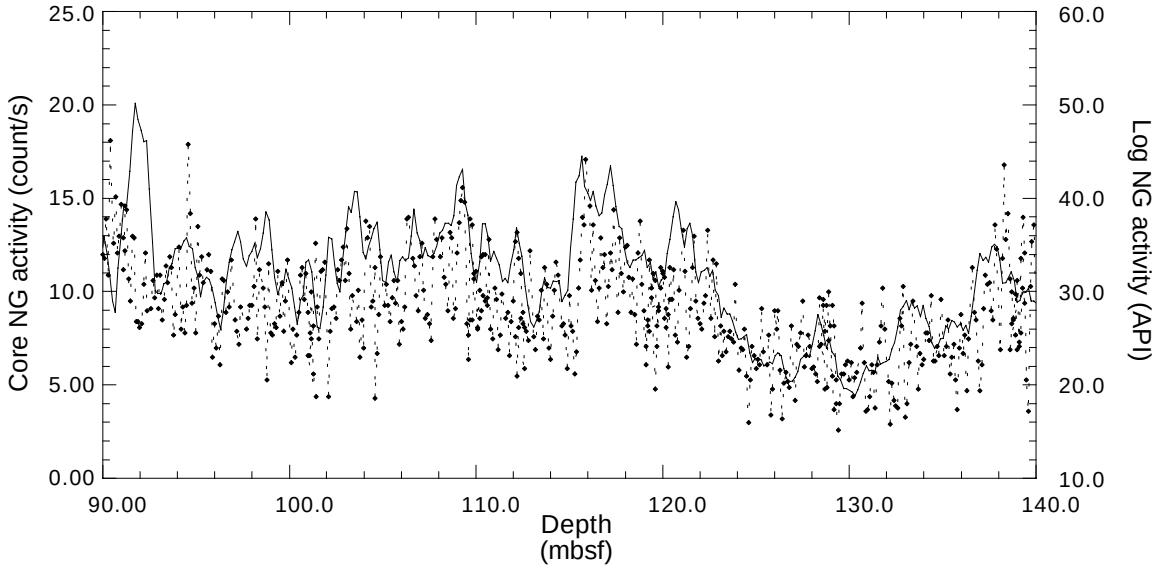

Figure 2. Comparison of uncorrected core-derived natural gamma (NG) data (in mbsf, dotted line) to log-derived natural gamma activity (solid line) from a portion of Site 926. These data illustrate the different resolutions of the two natural gamma instruments.

Table 1. Average sedimentation rates for the Pliocene–Pleistocene (0–5 Ma) portions of Sites 925–929.

Site	Average rate (cm/k.y.)
925	3.13
926	3.07
927	3.47
928	2.99
929	2.81

measurement, we have chosen to present background-corrected, core-derived natural gamma activity data in counts per second.

Decimeter-Scale Hole-to-Hole Correlations

At each site drilled during Leg 154, a composite depth scale was assembled for approximately the upper 300 m of section that related all of the multiple hole core data to a common depth scale. Although the composite depth scales, expressed in mcd (meters composite depth), significantly advanced shipboard science by providing a single, uninterrupted spliced record at each site, the shipboard composite depths only involved a simple depth-shifting of each core in each hole relative to the other cores (Curry, Shackleton, Richter, et al., 1995; Hagelberg et al., 1992). More accurate hole-to-hole correlations are required to relate multiple hole data to one another at a 10-cm (or better, as is the case for magnetic susceptibility) resolution (Fig. 3).

To compare data taken from adjacent holes at high resolution, it is necessary relate all data to a single depth scale that is accurate to the resolution of decimeters or greater. We accomplished this using the shipboard-generated splice as a reference for each site (Curry, Shackleton, Richter, et al., 1995). Although the choice of the shipboard splice is necessarily somewhat arbitrary, the sections of core selected for the splice were based on a quantitative and qualitative assessment of the amplitude and distortion of magnetic susceptibility oscillations from each hole at each site (Curry, Shackleton, Richter, et al., 1995). Using magnetic susceptibility as the primary hole-to-hole correlation tool, each core in each hole at each site (including Sites 925 and 927) was individually correlated to the corresponding interval of shipboard spliced magnetic susceptibility. In a previous study using a similar approach, inverse correlation methods (Martinson et al., 1982) were utilized to nonlinearly map GRAPE data from successive cores into the GRAPE spliced record (Hagelberg et al., 1995). However, because magnetic susceptibility data do not have the high sampling resolution that GRAPE data have, and also because magnetic susceptibility data is generally “spiky” in nature, inverse correlation methods were not appropriate for centimeter- to decimeter-scale hole-to-hole correlations. Instead, individual magnetic susceptibility features were correlated using linear correlations between measurements in cores from adjacent holes.

Correlation between the magnetic susceptibility data from each core to the shipboard magnetic susceptibility splice proceeded by first determining exactly what mcd depth in the shipboard splice corresponded to the top and bottom of each individual core. Because the shipboard composite depth scale only required the shifting of each core, the mcd scale could not always guide this determination. Individual magnetic susceptibility peaks and troughs in the splice and in each core were correlated until the correlation ceased to increase and was otherwise judged optimal. Intervals in which part of the individual core was used as the shipboard splice were common–these intervals were not changed in the correlation. This procedure was carried out for each core in the following sites: Site 925, 0–350 mcd; Site 926, 0–300 mcd; Site 927, 0–260 mcd; Site 928, 0–230 mcd; and Site 929, 0–150 mcd. Table 2 gives the correlation coefficient between each of these cores and the corresponding portion of the shipboard splice before and after this procedure. Figure 3 gives an example of the improvement in between-hole correlation that results from this procedure. The final correlation resulted in a transformation of mcd depths for each core in hole to the mcd of the shipboard splice. These transformed-to-splice mcd depths are referred to as revised meters composite depth, or rmcd.

Stacked Records

After correlation was complete, the magnetic susceptibility data on the rmcd scale were examined for any additional outliers or miscorrelations. The results were further checked and verified, where possible, using the natural gamma data. Correlations were repeated if necessary. When complete, the magnetic susceptibility and natural

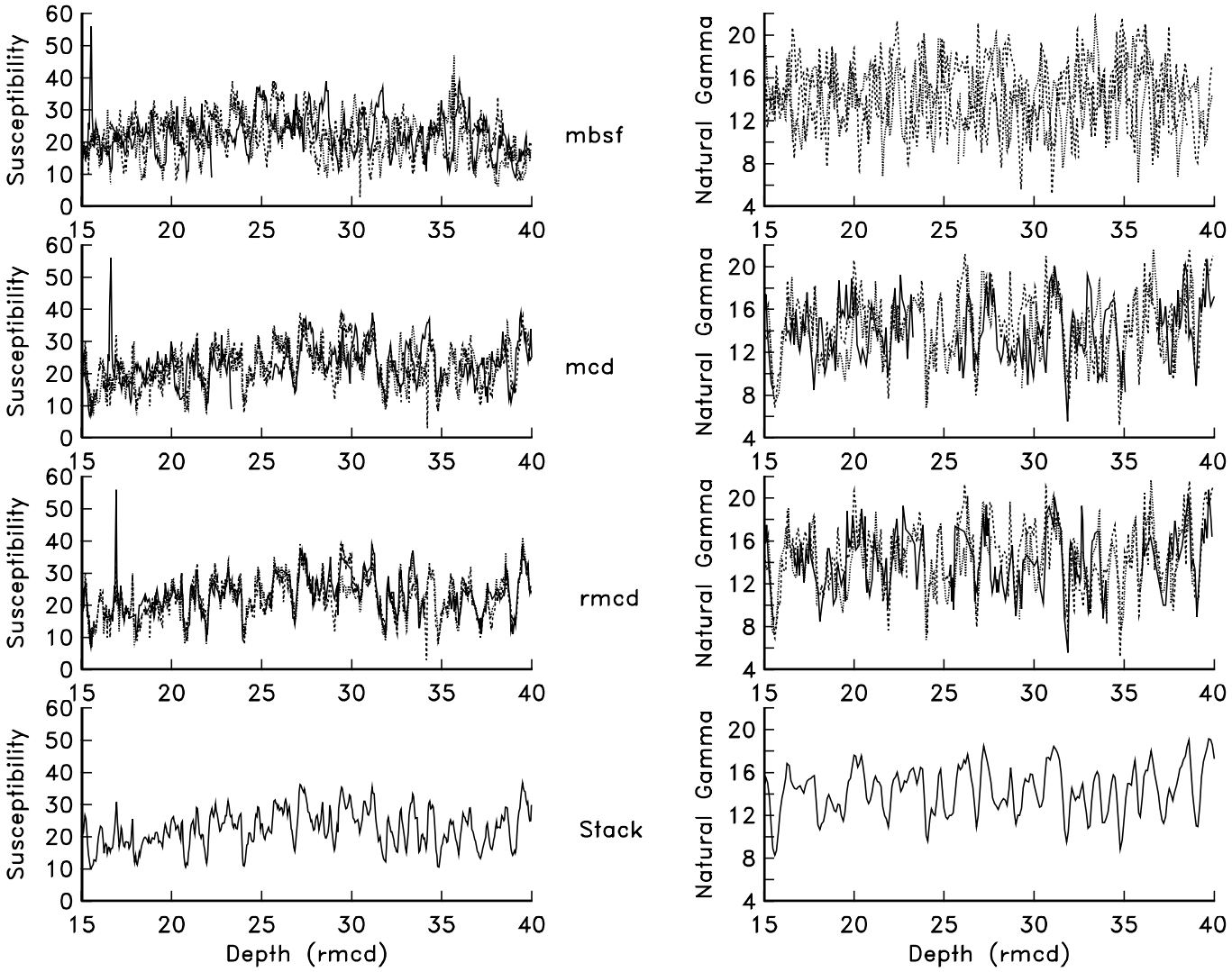

Figure 3. A portion of the magnetic susceptibility and natural gamma activity from the three holes drilled at Site 926. Data are presented in meters below seafloor (mbsf), meters composite depth (mcd), and revised meters composite depth (rmcd) scales. Stacked records (stack) were obtained by combining the multiple hole data (see text).

gamma activity data from the multiple holes at each site were combined, sorting according to the rmcd for each sample, into a single magnetic susceptibility and natural gamma record for each site. The combined multiple hole magnetic susceptibility data were then binned and smoothed, using a Gaussian interpolation scheme and a 15-cm window, to a uniform 5-cm sampling interval. The combined multiple hole natural gamma activity data were binned and smoothed to a uniform 10-cm sampling interval using a 30-cm Gaussian window. A portion of the resulting "stacked" magnetic susceptibility and natural gamma data from Site 926 is shown in Figure 3. Comparison of the stacked and smoothed data to the multiple hole data it was derived from qualitatively indicates the better signal-to-noise ratio and, hence, increased utility of the stacked data.

RESULTS

Stacked Natural Gamma Activity Records

Binned, smoothed, and stacked records of natural gamma activity for Sites 926, 928, and 929 are presented in Figures 4, 5, and 6, respectively. The binning and smoothing of the data allows error envelopes to be developed for each estimate because the multiple realizations from adjacent holes are combined in the stack. Thus, Figures 4–6 show a 1-standard deviation (1-σ) envelope about the total natural gamma-ray data. Although after correlation and binning, the number of samples in every sample bin is not constant, on average 2.5 measurements at Sites 926 and 928 were available within each 10-cm window. Because, on average 2.5 realizations were available for each sample, the random error in the stacked natural gamma-ray measurements is reduced by a factor of relative the individual measurements. Three measurements were available (on average) in the uppermost part of Site 929; likewise, the random error in the stacked measurements is on average reduced by a factor of. Because Gaussian windows were utilized in binning and smoothing, measurements from adjacent depths are also incorporated into the 1-σ calculation for each sample. These error envelopes provide much-needed constraints on subsequent lithologic interpretations that make use of natural gamma-ray measurements.

The stacked, smoothed natural gamma activity as well as magnetic susceptibility data are ideally suited for studies of lithologic composition on the Ceara Rise (e.g., King et al., this volume; Harris et al., this volume). Use of the stacked data allows the use of all data col-

Table 2. Correlation coefficient between each core and the shipboard splice reference before and after decimeter-scale correlation to the shipboard splice.

	Hole 925B APC cores		Hole 925D APC cores		Hole 925E APC cores	
Core	Before	After	Before	After	Before	After
1	0.885	0.945			0.575	0.919
2	–0.079	0.912			0.184	0.789
3	0.860	0.969			0.242	0.862
4	0.178	0.849			0.547	0.894
5	0.783	0.900				
6	0.596	0.786			0.184	0.510
7	0.028	0.532				
8	0.638	0.803				
9	0.602	0.893				
10	0.142	0.600				
11	0.176	0.664				
12	0.436	0.807	0.579	0.981		
13	0.294	0.733	0.242	0.975		
14	–0.040	0.685	0.349	0.867		
15	0.782	0.795	–0.015	0.990		
16	0.198	0.698	0.839	0.906		
17	0.728	0.923	0.919	0.957		
18	0.546	0.911	0.630	0.806		
19	0.469	0.939	0.542	0.823		
20	0.040	0.704	0.772	0.915		
21	0.055	0.751	0.745	0.902		
22	0.240	0.508	0.752	0.902		
23	0.798	0.908	0.523	0.687		
24	0.109	0.734	0.985	0.990		
25	–0.165	0.601	0.995	0.996		
26	0.235	0.808	0.986			
27	0.506	0.701	0.791	0.840		
28	0.267	0.330	0.256	0.769		
29	0.782	0.946	0.979	0.976		
30	0.822	0.916	0.907	0.982		
31	0.895	0.945	0.414	0.855		
32	0.844	0.969	0.584	0.900		
33	0.467	0.850	0.937	0.949		
34	0.896	0.998				

	Hole 926A APC cores		Hole 926B XCB cores		Hole 926C APC cores	
Core	Before	After	Before	After	Before	After
1	0.703	0.839	0.943	0.981	0.779	0.943
2	0.493	0.868	0.834	0.942	0.943	0.973
3	–0.020	0.760	0.892	0.945	0.822	0.960
4	0.149	0.892	0.811	0.885	0.803	0.891
5	0.276	0.902	0.776	0.915	0.861	0.947
6	0.312	0.617	0.721	0.905	0.865	0.978
7	0.329	0.883	0.738	0.893	0.960	0.964
8	0.710	0.918	0.636	0.889	0.795	0.904
9	0.853	0.927	0.161	0.775	0.841	0.939
10	0.593	0.696	0.709	0.890		
11	0.679	0.865	–0.149	0.713		
12	0.856	0.957	0.331	0.782		
13	0.265	0.753	0.898	0.939		
14	0.669	0.878	0.426	0.665		
15	0.031	0.767	0.912	0.947		
16	0.936	0.941	0.435	0.873		
17	0.200	0.901	0.622	0.914		
18	0.188	0.811	0.955	0.973		
19	0.332	0.830	0.964	0.986		
20	0.478	0.986	0.752	0.940		
21	0.549	0.876	0.665	0.872		
22	0.488	0.810	0.510	0.762		
23	0.896	0.910	0.583	0.787		
24	0.832	0.904	0.781	0.976		
25	0.877	0.965	0.885	0.964		
26	0.783	0.978	0.869	0.906		
27	–0.184	0.873	0.689	0.840		
28	0.795	0.897	0.207	0.680		
29	0.129	0.502	0.985	0.983		
30	0.135	0.511				

	Hole 927A APC cores		Hole 927B APC cores		Hole 927C APC, XCB cores	
Core	Before	After	Before	After	Before	After
1	0.285	0.687	0.310	0.837	–0.029	0.580
2	0.373	0.945	0.473	0.843	0.362	0.695
3	0.412	0.829	0.504	0.791	0.639	0.951
4	0.428	0.839	0.360	0.916	0.434	0.947
5	0.121	0.802	0.277	0.801	0.224	0.722
6	0.137	0.503	0.300	0.882	–0.048	0.784
7	0.108	0.433	0.126	0.738	0.149	0.931
8	0.279	0.723	0.405	0.837	0.256	0.890
9	0.135	0.825	0.180	0.860	0.312	0.474
10	0.281	0.872	0.501	0.745	0.357	0.847
11	0.134	0.675	0.326	0.689	0.173	0.546
12	0.271	0.795	0.125	0.661	0.561	0.836
13	0.270	0.785	0.271	0.918	–0.034	0.904
14	0.048	0.817	–0.027	0.651	0.266	0.777
15	0.181	0.581	–0.038	0.960	0.087	0.950
16	0.373	0.734	0.489	0.814	0.539	0.919
17	0.237	0.669	0.353	0.882	0.341	0.914
18	0.351	0.761	0.302	0.801	0.214	0.85
19	0.161	0.794	0.394	0.761		
20	0.040	0.302	0.253	0.812	0.210	0.86
21	0.181	0.592	0.246	0.583	0.229	0.86
22	0.188	0.681	0.376	0.551	0.123	0.762
23	0.896	0.910	0.583	0.787		
24	0.062	0.662	0.068	0.861	0.212	0.820
25	0.441	0.742	0.248	0.670	0.220	0.470
26	0.608	0.865	0.515	0.644	0.365	0.701
27	0.343	0.761	0.310	0.816	0.077	0.83
28	0.407	0.866	0.199	0.641	0.132	0.770
29	0.456	0.879				
30	0.145	0.876				
31	–0.346	0.272				

	Hole 928A APC, XBC cores		Hole 928B APC, XCB cores		Hole 928C APC, XCB cores	
Core	Before	After	Before	After	Before	After
1	0.561	0.878	0.385	0.834	0.279	0.687
2	0.264	0.664			0.262	0.899
3	0.501	0.929	0.119	0.634		
4	0.385	0.851	0.190	0.818	0.301	0.863
5	0.488	0.905	0.581	0.745	0.181	0.877
6	0.509	0.817	0.345	0.807	0.318	0.760
7	0.477	0.867	0.546	0.828	0.305	0.872
8	0.421	0.589	0.266	0.788	0.282	0.962
9	0.400	0.885	0.449	0.796	0.639	0.819
10	0.362	0.719	0.230	0.841	0.387	0.878
11	0.218	0.697	0.270	0.887	0.195	0.855
12	0.001	0.796	0.085	0.707	0.001	0.883
13	0.085	0.868	0.031	0.641	0.002	
14				0.378	0.916	0.295
15	0.245	0.777	0.451	0.886		
16	0.412	0.936			0.561	0.868
17	0.087	0.124	0.579	0.739		
18	0.539	0.881	0.683	0.892	0.393	0.828
19	0.353	0.759	0.366	0.517	0.595	0.801
20	0.401	0.761	0.571	0.681	0.562	0.776
21	0.306	0.720	0.715	0.936		
23	0.184	0.761				
25	0.476	0.767				

	Hole 929A APC cores		Hole 929B APC cores		Hole 929C APC cores	
Core	Before	After	Before	After	Before	After
1	0.310	0.820	0.468	0.896	0.378	0.865
2	0.094	0.865	0.746	0.896	0.254	0.745
3	0.275	0.788	0.375	0.901	0.313	0.967
4	0.381	0.871	0.467	0.907	0.341	0.905
5	0.254	0.831	0.276	0.975	0.318	0.773
6	0.062	0.859	0.355	0.904	0.073	0.743
7	0.208	0.916	0.698	0.884	0.330	0.854
8	0.066	0.545	0.272	0.964		
9	0.491	0.959	0.378	0.804	0.498	0.886
10	0.021	0.633	0.000	0.522	0.096	0.746
11	0.446	0.958	0.433	0.698	0.152	0.798
12	0.022	0.876	0.077	0.781	0.194	0.583
13	0.121	0.902	0.338	0.826	0.374	0.887
14			0.522	0.882		
15	0.577	0.790			0.762	0.906

	Hole 929D APC cores	
Core	Before	After
1	0.730	0.887
2	0.604	0.861
3	0.381	0.819
4	0.372	0.872
5	0.275	0.749
6	0.550	0.859

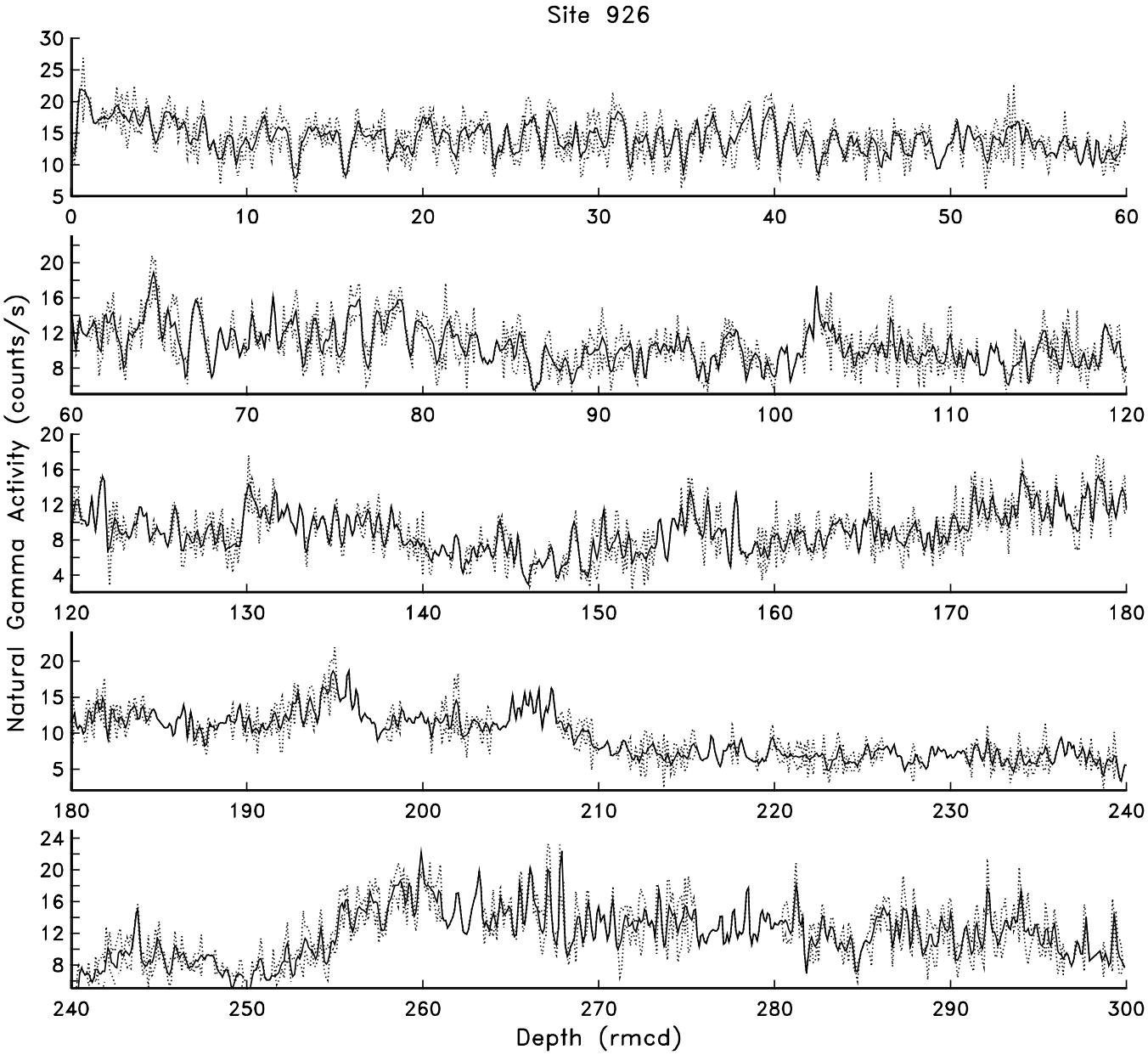

Figure 4. Natural gamma, Site 926; 1-σ envelopes are plotted with the stacked, interpolated natural gamma record.

lected from each site, rather than only a single (noisy) realization. In addition, the rmcd depth scale allows lithologic information collected in one hole to be transferred to the adjacent holes at each site at better than decimeter resolution.

The stacking procedure not only provides for less noisy (lower mean square error) estimates of total natural gamma-ray activity, but the multiple channels of natural gamma-ray emissions including the Th and K channels will also have reduced error. Typically, the Th and K channels are characterized by lower total activity and thus increased noisiness, complicating the use of core-derived measurements of these variables. (Note: The K gamma-ray activity refers to the 1100–1590 keV energy range and the Th gamma-ray activity refers to the 2000–3000 keV energy range, the channels used for both downhole and sediment measurements during Leg 154). Because the stacking procedure allows for an averaging of multiple Th and K channel natural gamma-ray activity in each 10-cm bin, the core-derived measurements of Th and K natural gamma-ray activity will also have lower random error, as discussed for the total natural gamma-ray activity above. In Figures 7, 8, and 9, the binned and stacked total natural gamma activity, Th and K natural gamma activity are displayed for Sites 926, 928, and 929, respectively. These core-derived natural gamma activity data are now ideally suited for comparison to mineralogy and for examination of Th and K activity changes on orbital time scales; they are also superior data for integration with downhole logs (e.g., deMenocal and King, 1995). Additional investigation using these data will allow compositional changes in terrigenous sedimentation on the Ceara Rise to be quantitatively evaluated.

Core and Log Integration

Integration of the core- and log-derived natural gamma-ray activity data follows naturally from the above result. Once the core-derived and log-derived data sets are integrated, the core-based age control and geochemical information can be transferred directly to the

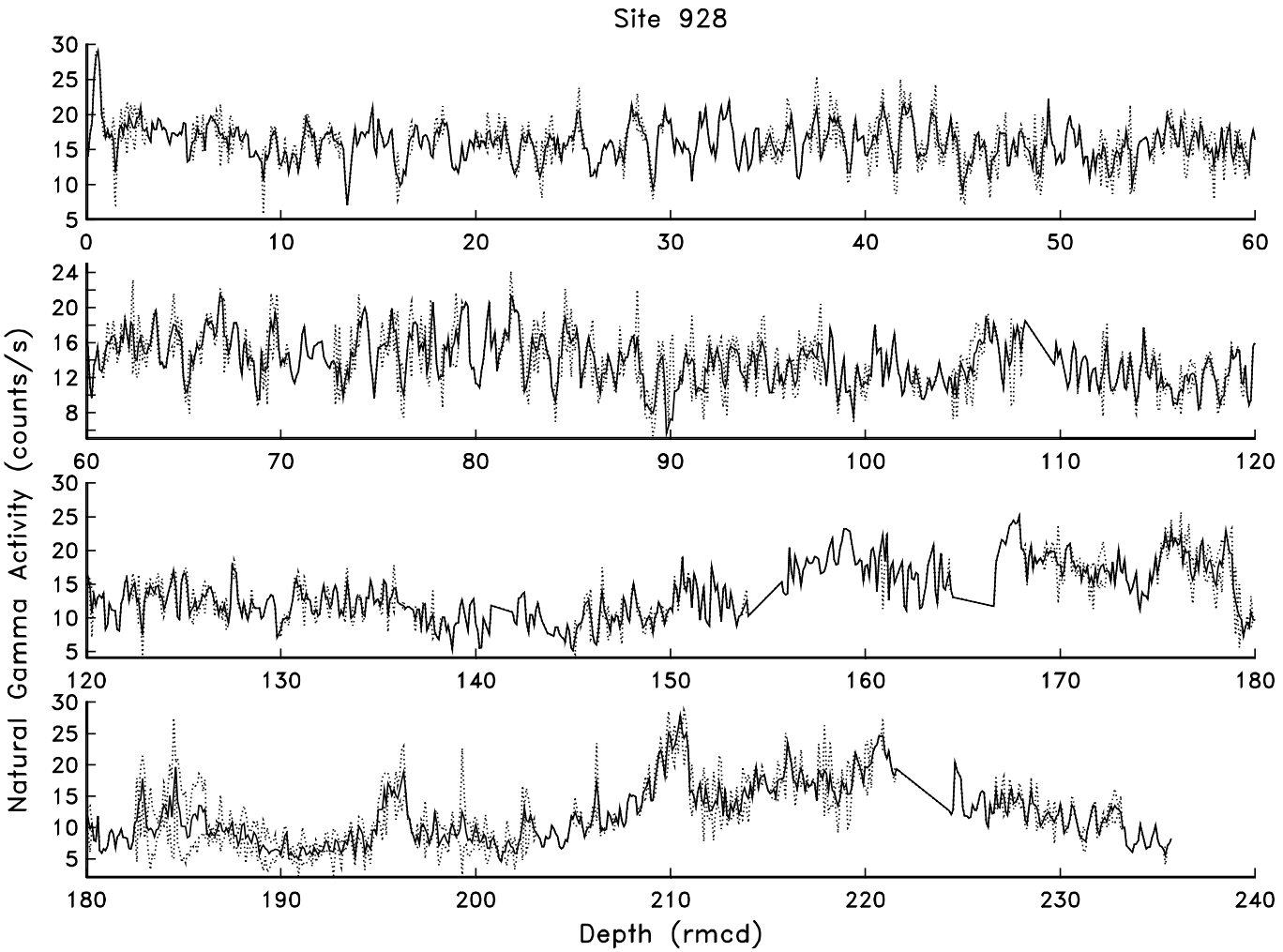

Figure 5. Natural gamma, Site 928; 1-σ envelopes are plotted with the stacked, interpolated natural gamma record.

downhole logs; similarly, log-derived information can be transferred to the actual cored material. Investigations can also be made into the empirical vertical and temporal resolution of both the core and the log data (e.g., deMenocal and King, 1995). Integration can only occur if the two data sets must be related to a common depth scale. As Figure 10A shows, although post-cruise depth shifting relates the log-derived natural gamma activity to the mbsf depth scale, the log-derived data now need to be related to the rmcd depth scale (or vice versa, as long as a common depth scale is achieved).

An example from Site 926 illustrates integration of the core and log depth scales (Fig. 10). In Figure 10A, core- and log-derived total natural gamma-ray data from Site 926 are displayed on rmcd and mbsf depth scales, respectively. Transfer of the core-derived data to the rmcd depth scale is described earlier in the text; depth-shifting of the log-derived data to mbsf depth is provided post-cruise by the Borehole Research Group (Curry, Shackleton, Richter, et al., 1995). In the bottom panel, the two records have been correlated to one another and related to a common depth scale (rmcd depth) through the use of inverse correlation methods (Martinson et al., 1982).

The inverse correlation procedure that relates the two depth scales is as follows: tie points, features that are equivalent in the core and the log records for the top (56.10 rmcd, core; 50.13 mbsf, log) and bottom (306.71 rmcd, core; 276.90 mbsf, log) of the core and log data that will be correlated are identified. From an initial correlation coefficient between the two signals of 0.48, inverse mapping of a Fourier sine series proceeds iteratively until the correlation ceases to increase without inducing unrealistic, discontinuous distortions to the mapping function and the data. A final correlation of 0.654 was achieved with 72 coefficients of the Fourier mapping function. The mapping function relating Site 926 log data (on mbsf) to the rmcd scale is given in Table 3 and displayed in Figure 11.

Once related to the same common depth scale, the astronomically calibrated age model developed by Shackleton et al. (this volume) can be transferred to the log data, and thus the core and log data can be compared in either the time or the depth domain. To investigate the temporal variability in terrigenous sedimentation at the Ceara Rise, as well as to determine empirically the effective temporal resolution of the logging measurements, it is useful to view the natural gamma core and log activity in the time domain. Figure 12 shows the Site 926 log-derived and core-derived natural gamma-ray activity converted to age using the time scale of Shackleton et al. (this volume). Both natural gamma-ray activity records document a long-term evolution, with a major decrease after 11 Ma, followed by an increase near 8 Ma. Evidence for orbital scale variations is discernible in both records as well.

The natural gamma-ray activity oscillations documented by the core and log measurements are quantified by examination in the frequency domain. In Figure 13, we give the power spectra, the coherence spectrum and the gain spectrum for the Site 926 log and core natural gamma activity records over the entire 1.8–14 m.y. interval

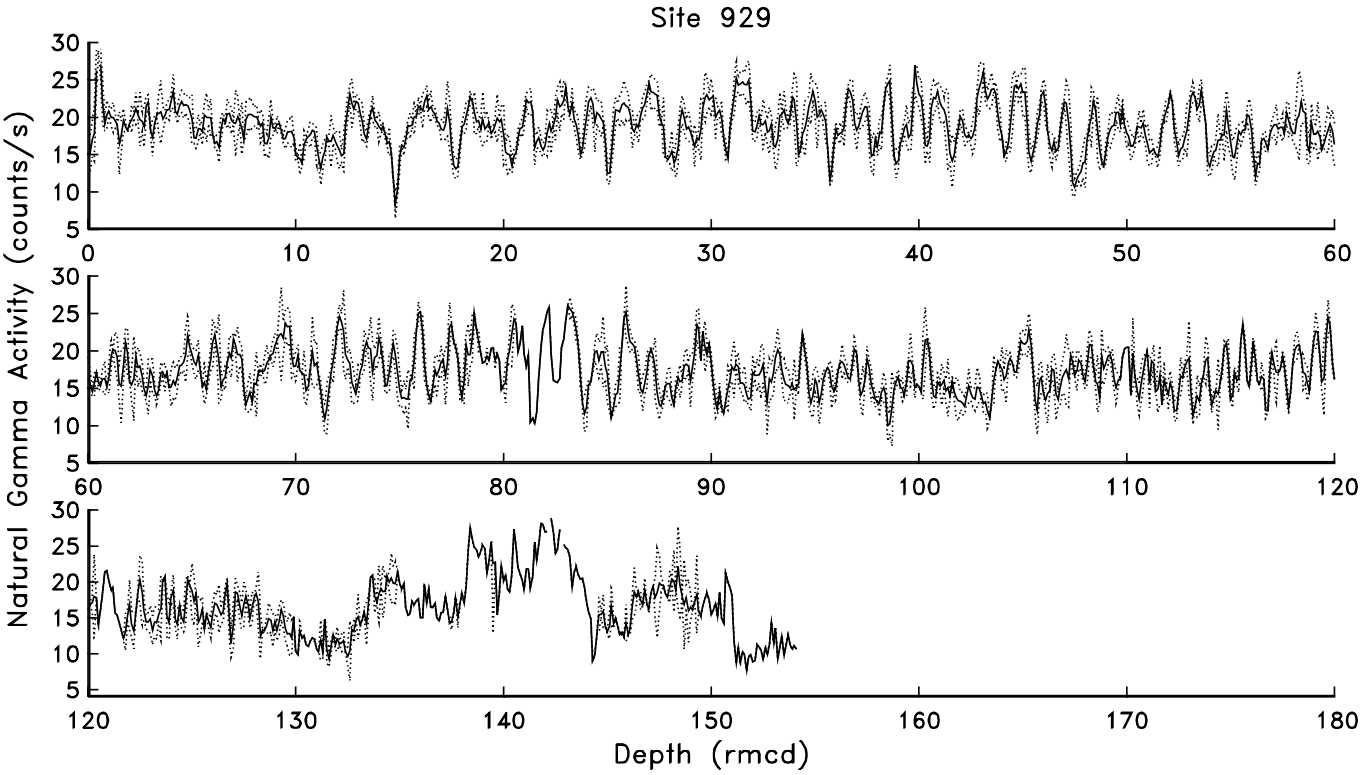

Figure 6. Natural gamma, Site 929; 1-σ envelopes are plotted with the stacked, interpolated natural gamma record.

represented by the integrated data. Typically, paleoclimatic time series investigations involve spectral analysis of no more than a few m.y. at most; the records displayed in Figure 13 represent over 10 m.y. As a result, the low frequency oscillations that are typically difficult to see in paleoclimatic records are observed in both the core and the log natural gamma activity records. In particular, concentrations of variance are observed at periods of 412 k.y., 123 k.y., and 96 k.y. These oscillations are part of the primary Milankovitch forcing (e.g., as described by Berger, 1988). Typically, the 412-k.y. eccentricity oscillation is difficult to detect, owing to insufficient record length and resolution, although in theory the 412-k.y. oscillation is higher in amplitude than the 100-k.y. components of eccentricity (Berger, 1988). Likewise, the ~96-k.y. and ~123-k.y. oscillations that are typically not separated in the frequency domain are commonly known, together, as the well-known "100-k.y." concentration of variance (e.g., Imbrie et al., 1992). Both core and log data demonstrate a strong concentration of variance at 41 k.y., which corresponds to obliquity variations. Because the log data are not high enough in resolution to document changes in the orbital precession band (23 k.y.–19 k.y.) without aliasing, only variance to 41 k.y. is displayed. However, were the core-derived data plotted to the effective Nyquist frequency of ~10 k.y., statistically significant precession-band variance would be evident, although reduced in comparison to the variance at longer periods (>100 k.y.).

Both core and log natural gamma records are significantly coherent at these orbital frequencies, as well as most frequencies lower than 100 k.y.$^{-1}$. Both records are in phase (not shown), with an average phase equal to 0 at every frequency. The gain function (Fig. 13, bottom panel), identifies the extent to which log-derived natural gamma-ray activity may be attenuated and/or amplified relative to stacked core-derived measurements. The gain function quantifies the amount of amplification/attenuation as a function of the coherent variance shared between the two measurements. For any frequency f, the gain factor of the log-derived measurements over the core-derived measurements, $\hat{H}(f)$, is calculated as the magnitude of the cross-spectrum between the core and log data at frequency f, ($|\hat{G}_{xy}(f)|$, where x = log data and y = core data) normalized by the amplitude of the log spectrum, $\hat{G}_{xx}(f)$ (Bendat and Piersol, 1986):

$$\hat{H}(f) = \frac{|\hat{G}_{xy}(f)|}{\hat{G}_{xx}(f)}.$$

The gain function for the Site 926 log/core comparison indicates that at almost every frequency, the log natural gamma record is attenuated (lower in amplitude) relative to the core. The only exception is the 41-k.y. cycle. As suggested by the power spectra plot, the amplitude of the 41-k.y. cycle recorded in the log natural gamma data is strongly amplified relative to the amplitude recorded in the core data. This may be a consequence of the higher continuity of the log data relative to the core data. Additional factors contributing to the amplification of the log measurements are under continued study. From the example given here, however, one can conclude that both core and log natural gamma activity data from Site 926 accurately document orbital to tectonic scale variability in terrigenous sedimentation.

CONCLUSIONS

Using magnetic susceptibility as a correlation tool, natural gamma activity data measured in adjacent holes at Ceara Rise Sites 926, 928, and 929 were combined together to produce a superior record for each site. In the process of correlating data from adjacent holes to the scale of decimeters, a revised composite depth scale is developed that permits integration of multiple hole data at very high resolution. As a result of application of the methods discussed above, "stacked" records of natural gamma and magnetic susceptibility were developed that were less noisy at all channels and that had lower mean

square error. These high-quality natural gamma data, which make use of all available measurements, are more robust than is typically available from a single APC/XCB hole. Like downhole log measurements of natural gamma emissions, these multichannel measurements provide quantitative information regarding the composition of terrigenous materials deposited on the Ceara Rise. These data are ideal for the integration of core and log natural gamma variability in those intervals in which multiple hole data and logs coexist. An example is given using the Site 926 log- and core-derived natural gamma activity records. It is demonstrated that although core and log natural gamma data record similar long term variations, log data generally record lower amplitude variations than the core data. Additional investigation using these data will allow compositional changes in terrigenous sedimentation on the Ceara Rise to be quantitatively evaluated.

REFERENCES

Bendat, J.S., and Piersol, A.G., 1988. *Random Data: Analysis and Measurement Procedures:* New York (Wiley).

Berger, A., 1988. Milankovitch theory and climate. *Rev. Geophys.*, 26:624–657.

Curry, W.B., Shackleton, N.J., Richter, C., et al., 1995. *Proc. ODP, Init. Repts.*, 154: College Station, TX (Ocean Drilling Program).

deMenocal, P., and King. T., 1995. Paleoclimate information from sediments and downhole logs, I: chronostratigraphic applications. *Proc. 5th Int. Conf. Paleoceanogr.*, Halifax, 38–39.

Fertl, W.H., 1979. Gamma ray spectral data assists in complex formation evaluation. *Log Analyst*, 20:421–423.

Hagelberg, T., Shackleton, N., Pisias, N., and Shipboard Scientific Party, 1992. Development of composite depth sections for Sites 844 through 854. *In* Mayer, L., Pisias, N., Janecek, T., et al., *Proc. ODP, Init. Repts.*, 138 (Pt. 1): College Station, TX (Ocean Drilling Program), 79–85.

Hagelberg, T.K., Pisias, N.G., Shackleton, N.J., Mix, A.C., and Harris, S., 1995. Refinement of a high-resolution, continuous sedimentary section for studying equatorial Pacific Ocean paleoceanography, Leg 138. *In* Pisias, N.G., Mayer, L.A., Janecek, T.R., Palmer-Julson, A., and van Andel, T.H. (Eds.), *Proc. ODP, Sci Results*, 138: College Station, TX (Ocean Drilling Program), 31–46.

Harris, S., Hagelberg, T., Mix, A., Pisias, N.G., and Shackleton, N.J., 1995. Sediment depths determined by comparisons of GRAPE and logging density data during Leg 138. *In* Pisias, N.G., Mayer, L.A., Janecek, T.R., Palmer-Julson, A., and van Andel, T.H. (Eds.), *Proc. ODP, Sci. Results*, 138: College Station, TX (Ocean Drilling Program), 47–57.

Hoorn, C., Guerrero, J., Sarmiento, G. A., and Lorente, M.A., 1995. Andean tectonics as a cause for changing drainage patterns in Miocene northern South America. *Geology*, 23:237–240.

Hoppie, B.W., Blum, P., and the Shipboard Scientific Party, 1994. Natural gamma-ray measurements on ODP cores: introduction to procedures with examples from Leg 150. *In* Mountain, G.S., Miller, K.G., Blum, P., et al., *Proc. ODP, Init. Repts.*, 150: College Station, TX (Ocean Drilling Program), 51–59.

Imbrie, J., Boyle, E.A., Clemens, S.C., Duffy, A., Howard, W.R., Kukla, G., Kutzbach, J., Martinson, D.G., McIntyre, A., Mix, A.C., Molfino, B., Morley, J.J., Peterson, L.C., Pisias, N.G., Prell, W.L., Raymo, M.E., Shackleton, N.J., and Toggweiler, J.R., 1992. On the structure and origin of major glaciation cycles, 1. Linear responses to Milankovitch forcing. *Paleoceanography*, 7:701–738.

Lyle, M., Bristow, J., Bloemendahl, J., and Rack, F., in press. Comparison of natural gamma activity profiles from downhole logging and the MST core logger at ODP Site 911 (Yermak Plateau). *In* Thiede, J., Myhre, A.M., and Firth, J.V., Johnson, G.L., and Ruddiman, W.F. (Eds.), *Proc. ODP, Sci. Results*, 151: College Station, TX (Ocean Drilling Program).

Martinson, D.G., Menke, W., and Stoffa, P.L., 1982. An inverse approach to signal correlation. *J. Geophys. Res.*, 87:4807–4818.

Pisias, N.G., and Mix, A.C., 1988. Aliasing of the geologic record and the search for long-period Milankovitch cycles. *Paleoceanography*, 3:613–619.

Ms 154SR-140
Date of initial receipt: 30 November 1995
Date of acceptance: 16 April 1996

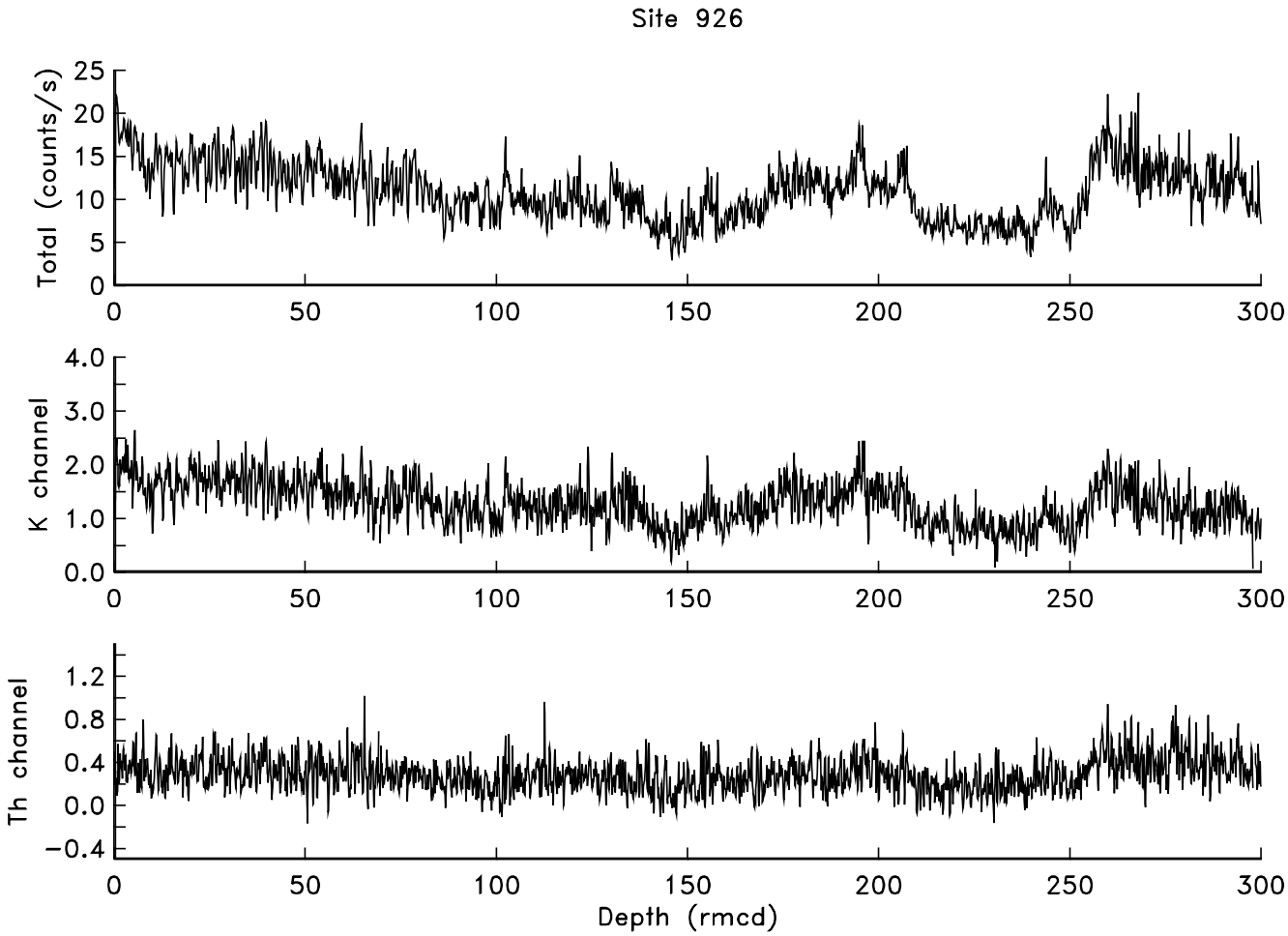

Figure 7. Total natural gamma activity, K-channel natural gamma activity, and Th-channel natural gamma activity, Site 926.

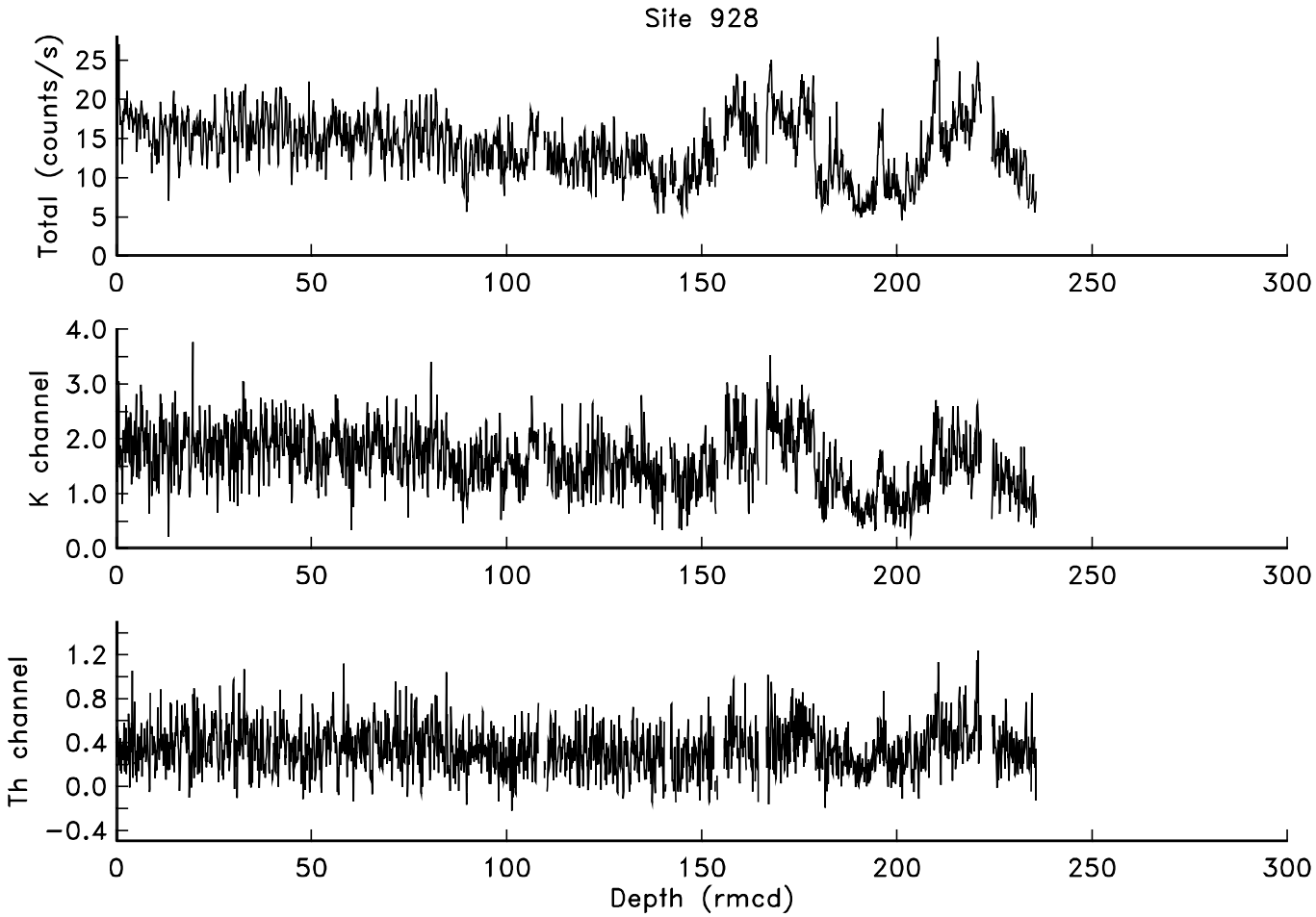

Figure 8. Total natural gamma activity, K-channel natural gamma activity, and Th-channel natural gamma activity, Site 928.

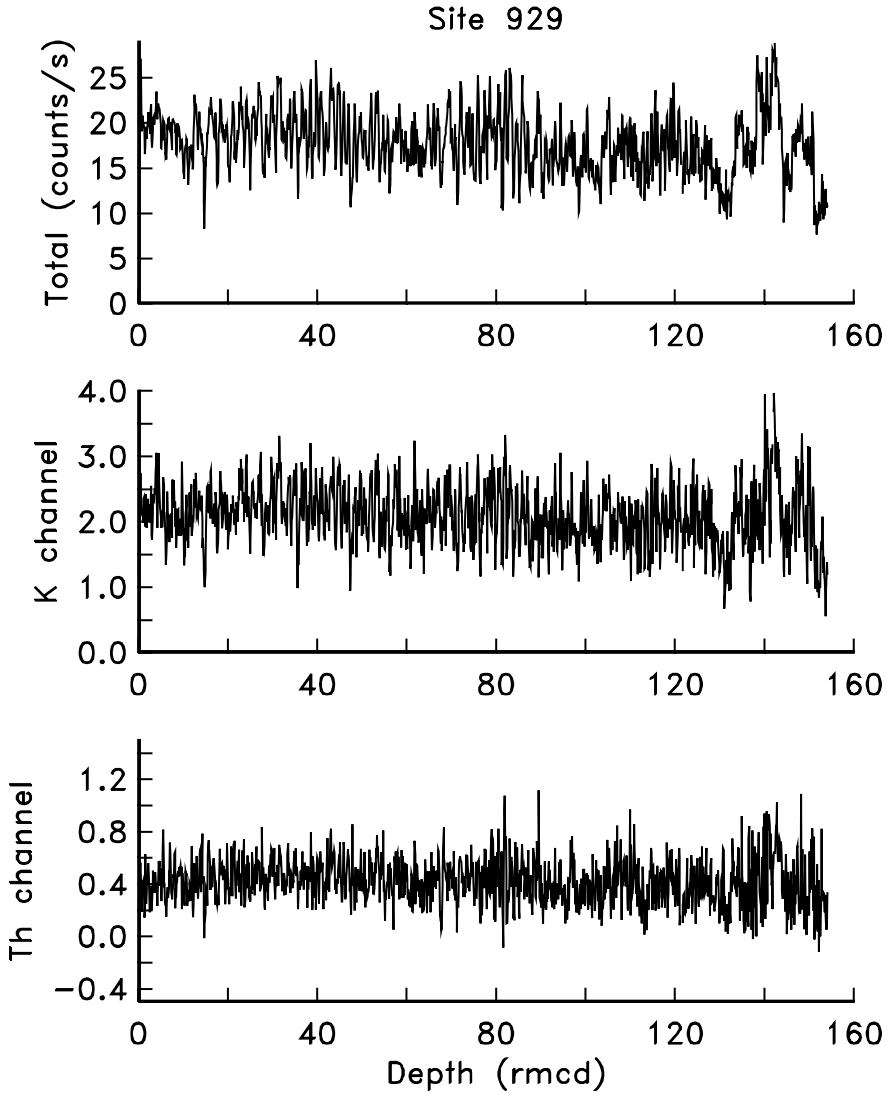

Figure 9. Total natural gamma activity, K-channel natural gamma activity, and Th-channel natural gamma activity, Site 929.

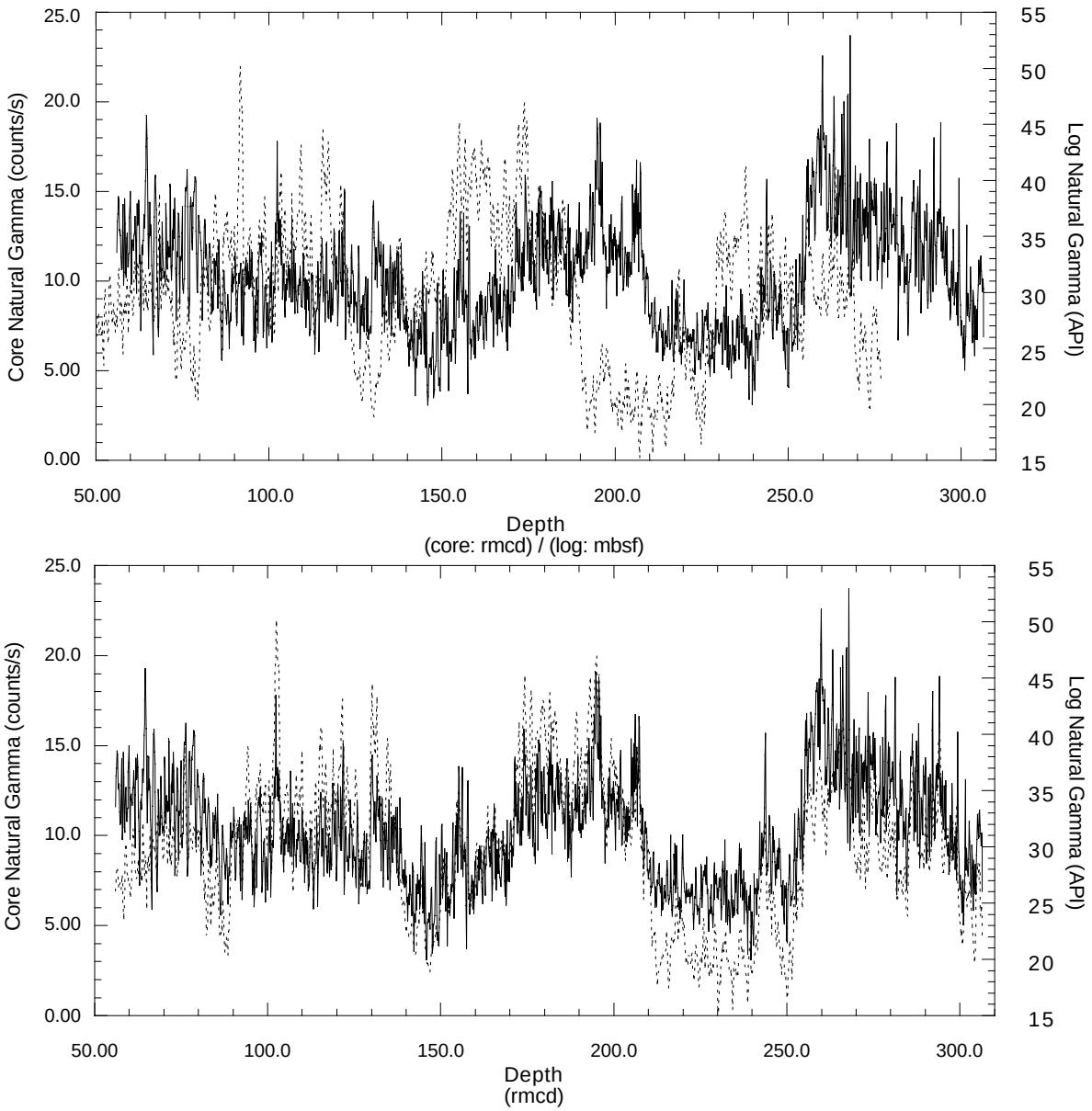

Figure 10. Site 926 core-derived natural gamma activity stack (solid line) compared to the log-derived natural gamma activity record (dashed line). Top: before mapping log MBSF depths to core rmcd depths. Bottom: after mapping.

Table 3. Mapping function relating Site 926 log-derived natural gamma activity recorded in mbsf depths (left) to the equivalent rmcd depths (right).

926B log (mbsf)	926B (rmcd)	926B log (mbsf)	926B (rmcd)	926B log (mbsf)	926B (rmcd)	926B log (mbsf)	926B (rmcd)
50.14	56.10	57.61	64.86	65.07	72.16	72.54	81.93
50.29	56.26	57.76	64.99	65.23	72.30	72.69	82.05
50.44	56.42	57.91	65.12	65.38	72.43	72.85	82.18
50.60	56.57	58.06	65.25	65.53	72.57	73.00	82.30
50.75	56.74	58.22	65.38	65.68	72.71	73.15	82.43
50.90	56.90	58.37	65.51	65.84	72.85	73.30	82.55
51.05	57.06	58.52	65.64	65.99	72.99	73.46	82.66
51.21	57.23	58.67	65.77	66.14	73.14	73.61	82.78
51.36	57.40	58.83	65.91	66.29	73.28	73.76	82.90
51.51	57.58	58.98	66.05	66.45	73.44	73.91	83.02
51.66	57.76	59.13	66.19	66.60	73.59	74.07	83.13
51.82	57.95	59.28	66.33	66.75	73.76	74.22	83.25
51.97	58.14	59.44	66.47	66.90	73.92	74.37	83.37
52.12	58.33	59.59	66.62	67.06	74.10	74.52	83.48
52.27	58.53	59.74	66.77	67.21	74.28	74.68	83.60
52.43	58.74	59.89	66.92	67.36	74.47	74.83	83.72
52.58	58.96	60.05	67.07	67.51	74.67	74.98	83.84
52.73	59.17	60.20	67.23	67.67	74.88	75.13	83.96
52.88	59.40	60.35	67.39	67.82	75.10	75.29	84.08
53.04	59.62	60.50	67.55	67.97	75.33	75.44	84.20
53.19	59.86	60.66	67.71	68.12	75.57	75.59	84.32
53.34	60.09	60.81	67.88	68.28	75.83	75.74	84.45
53.49	60.32	60.96	68.05	68.43	76.09	75.90	84.58
53.64	60.55	61.11	68.22	68.58	76.36	76.05	84.71
53.80	60.78	61.26	68.38	68.73	76.64	76.20	84.84
53.95	61.00	61.42	68.55	68.88	76.93	76.35	84.98
54.10	61.22	61.57	68.72	69.04	77.22	76.50	85.12
54.25	61.44	61.72	68.89	69.19	77.51	76.66	85.26
54.41	61.65	61.87	69.06	69.34	77.80	76.81	85.40
54.56	61.85	62.03	69.23	69.49	78.08	76.96	85.55
54.71	62.04	62.18	69.39	69.65	78.36	77.11	85.70
54.86	62.23	62.33	69.56	69.80	78.63	77.27	85.85
55.02	62.41	62.48	69.72	69.95	78.89	77.42	86.01
55.17	62.59	62.64	69.88	70.10	79.13	77.57	86.17
55.32	62.76	62.79	70.03	70.26	79.37	77.72	86.33
55.47	62.92	62.94	70.19	70.41	79.60	77.88	86.50
55.63	63.08	63.09	70.34	70.56	79.81	78.03	86.67
55.78	63.23	70.93	71.17	80.58	78.64	87.38	63.27
56.39	63.81	63.86	71.07	71.32	80.75	78.79	87.56
56.54	63.95	64.01	71.21	71.48	80.92	78.94	87.75
56.69	64.08	64.16	71.35	71.63	81.08	79.10	87.94
56.85	64.22	64.31	71.49	71.78	81.23	79.25	88.13
57.00	64.35	64.47	71.62	71.93	81.38	79.40	88.32
57.15	64.48	64.62	71.76	72.09	81.52	79.55	88.52
57.30	64.61	64.77	71.89	72.24	81.66	79.71	88.72
57.45	64.73	64.92	72.03	72.39	81.79	79.86	88.91

926B log (mbsf)	926B (rmcd)	926B log (mbsf)	926B (rmcd)	926B log (mbsf)	926B (rmcd)	926B log (mbsf)	926B (rmcd)
80.01	89.11	87.48	97.37	94.95	106.01	102.41	114.20
80.16	89.31	87.63	97.54	95.10	106.16	102.57	114.37
80.31	89.51	87.78	97.71	95.25	106.32	102.72	114.55
80.47	89.71	87.93	97.88	95.40	106.47	102.87	114.72
80.62	89.90	88.09	98.05	95.55	106.62	103.02	114.89
80.77	90.10	88.24	98.22	95.71	106.77	103.17	115.07
80.92	90.29	88.39	98.40	95.86	106.92	103.33	115.24
81.08	90.48	88.54	98.58	96.01	107.07	103.48	115.41
81.23	90.67	88.70	98.76	96.16	107.22	103.63	115.58
81.38	90.86	88.85	98.94	96.32	107.37	103.78	115.75
81.53	91.05	89.00	99.12	96.47	107.52	103.94	115.93
81.69	91.23	89.15	99.30	96.62	107.67	104.09	116.10
81.84	91.41	89.31	99.48	96.77	107.82	104.24	116.26
81.99	91.59	89.46	99.67	96.93	107.97	104.39	116.43
82.14	91.77	89.61	99.85	97.08	108.12	104.55	116.60
82.30	91.94	89.76	100.04	97.23	108.28	104.70	116.77
82.45	92.12	89.92	100.23	97.38	108.43	104.85	116.94
82.60	92.29	90.07	100.42	97.54	108.59	105.00	117.10
82.75	92.45	90.22	100.61	97.69	108.74	105.16	117.27
82.91	92.62	90.37	100.79	97.84	108.90	105.31	117.44
83.06	92.79	90.53	100.98	97.99	109.06	105.46	117.60
83.21	92.95	90.68	101.17	98.15	109.22	105.61	117.77
83.36	93.11	90.83	101.36	98.30	109.39	105.77	117.93
83.52	93.27	90.98	101.55	98.45	109.56	105.92	118.10
83.67	93.43	91.14	101.74	98.60	109.72	106.07	118.26
83.82	93.59	91.29	101.93	98.76	109.89	106.22	118.42
83.97	93.75	91.44	102.12	98.91	110.07	106.38	118.59
84.12	93.91	91.59	102.30	99.06	110.24	106.53	118.75
84.28	94.06	91.74	102.49	99.21	110.42	106.68	118.92
84.43	94.22	91.90	102.67	99.36	110.95	107.14	119.40
84.89	94.68	92.35	103.21	99.82	111.13	107.29	119.57
85.04	94.83	92.51	103.39	99.97	111.32	107.44	119.73
85.19	94.99	92.66	103.57	100.13	111.50	107.59	119.89
85.34	95.14	92.81	103.74	100.28	111.68	107.75	120.05
85.50	95.29	92.96	103.91	100.43	111.86	107.90	120.21
85.65	95.45	93.12	104.08	100.58	112.05	108.05	120.37
85.80	95.60	93.27	104.25	100.74	112.23	108.20	120.53
85.95	95.76	93.42	104.42	100.89	112.41	108.36	120.70

926B log (mbsf)	926B (rmcd)	926B log (mbsf)	926B (rmcd)	926B log (mbsf)	926B (rmcd)	926B log (mbsf)	926B (rmcd)
86.11	95.91	93.57	104.58	101.04	112.59	108.51	120.86
86.26	96.07	93.73	104.75	101.19	112.77	108.66	121.02
86.41	96.23	93.88	104.91	101.35	112.95	108.81	121.18
86.56	96.39	94.03	105.07	101.50	113.13	108.97	121.34
86.72	96.55	94.18	105.23	101.65	113.31	109.12	121.50
86.87	96.71	94.34	105.39	101.80	113.49	109.27	121.66
87.02	96.87	94.49	105.55	101.96	113.67	109.42	121.83
87.17	97.03	94.64	105.70	102.11	113.84	109.58	121.99
87.33	97.20	94.79	105.86	102.26	114.02	109.73	122.16

926B log (mbsf)	926B (rmcd)	926B log (mbsf)	926B (rmcd)	926B log (mbsf)	926B (rmcd)	926B log (mbsf)	926B (rmcd)
109.88	122.33	117.35	131.61	124.82	139.93	132.28	149.66
110.03	122.51	117.50	131.73	124.97	140.13	132.44	149.87
110.19	122.68	117.65	131.85	125.12	140.34	132.59	150.07
110.34	122.86	117.81	131.97	125.27	140.54	132.74	150.28
110.49	123.05	117.96	132.09	125.43	140.74	132.89	150.47
110.64	123.24	118.11	132.21	125.58	140.94	133.05	150.66
110.79	123.43	118.26	132.34	125.73	141.14	133.20	150.85
110.95	123.63	118.41	132.46	125.88	141.33	133.35	151.03
111.10	123.84	118.57	132.59	126.03	141.53	133.50	151.21
111.25	124.05	118.72	132.71	126.19	141.72	133.65	151.39
111.40	124.26	118.87	132.84	126.34	141.91	133.81	151.56
111.56	124.49	119.02	132.97	126.49	142.11	133.96	151.72
111.71	124.72	119.18	133.11	126.64	142.29	134.11	151.89
111.86	124.95	119.33	133.24	126.80	142.48	134.26	152.04
112.01	125.19	119.48	133.38	126.95	142.67	134.42	152.20
112.17	125.44	119.63	133.52	127.10	142.85	134.57	152.35
112.32	125.69	119.79	133.66	127.25	143.03	134.72	152.50
112.47	125.94	119.94	133.81	127.41	143.22	134.87	152.65
112.62	126.20	120.09	133.96	127.56	143.40	135.03	152.79
112.78	126.45	120.24	134.12	127.71	143.58	135.18	152.93
112.93	126.71	120.40	134.27	127.86	143.76	135.33	153.07
113.08	126.96	120.55	134.43	128.02	143.94	135.48	153.21
113.23	127.22	120.70	134.59	128.17	144.12	135.64	153.35
113.39	127.46	120.85	134.76	128.32	144.31	135.79	153.48
113.54	127.70	121.01	134.93	128.47	144.49	135.94	153.62
113.69	127.93	121.16	135.11	128.63	144.67	136.09	153.75
113.84	128.15	121.31	135.28	128.78	144.86	136.25	153.88
114.00	128.37	121.46	135.47	128.93	145.05	136.40	154.02
114.15	128.58	121.62	135.65	129.08	145.24	136.55	154.15
114.30	128.77	121.77	135.84	129.24	145.43	136.70	154.28
114.45	128.96	121.92	136.03	129.39	145.62	136.86	154.41
114.60	129.14	122.07	136.22	129.54	145.82	137.01	154.55
114.76	129.32	122.22	136.42	129.69	146.02	137.16	154.68
114.91	129.48	122.38	136.62	129.84	146.22	137.31	154.82
115.06	129.64	122.53	136.82	130.00	146.42	137.46	154.95
115.21	129.80	122.68	137.02	130.15	146.63	137.62	155.09
115.37	129.95	122.83	137.23	130.30	146.84	137.77	155.23
115.52	130.09	122.99	137.43	130.45	147.05	137.92	155.37
115.67	130.23	123.14	137.64	130.61	147.26	138.07	155.51
115.82	130.37	123.29	137.85	130.76	147.48	138.23	155.66
115.98	130.50	123.44	138.06	130.91	147.70	138.38	155.80
116.13	130.63	123.60	138.27	131.06	147.92	138.53	155.95
116.28	130.76	123.75	138.48	131.22	148.14	138.68	156.10
116.43	130.88	123.90	138.68	131.37	148.36	138.84	156.26
116.59	131.01	124.05	138.89	131.52	148.58	138.99	156.41
116.74	131.13	124.21	139.10	131.67	148.80	139.14	156.57
116.89	131.25	124.36	139.31	131.83	149.02	139.29	156.73
117.04	131.37	124.51	139.52	131.98	149.24	139.45	156.90
117.20	131.49	124.66	139.72	132.13	149.45	139.60	157.07

926B log (mbsf)	926B (rmcd)	926B log (mbsf)	926B (rmcd)	926B log (mbsf)	926B (rmcd)	926B log (mbsf)	926B (rmcd)
139.75	157.24	147.22	165.57	154.69	174.01	162.15	182.02
139.90	157.41	147.37	165.75	154.84	174.14	162.31	182.14
140.06	157.59	147.52	165.93	154.99	174.28	162.46	182.26
140.21	157.77	147.68	166.12	155.14	174.42	162.61	182.37
140.36	157.96	147.83	166.32	155.30	174.56	162.76	182.50
140.51	158.14	147.98	166.52	155.45	174.71	162.92	182.62
140.67	158.33	148.13	166.72	155.60	174.86	163.07	182.75
140.82	158.52	148.29	166.93	155.75	175.02	163.22	182.88
140.97	158.71	148.44	167.15	155.91	175.19	163.37	183.01
141.12	158.90	148.59	167.37	156.06	175.36	163.53	183.15
141.27	159.10	148.74	167.60	156.21	175.54	163.68	183.30
141.43	159.29	148.89	167.83	156.36	175.73	163.83	183.45
141.58	159.49	149.05	168.06	156.51	175.92	163.98	183.61
141.73	159.68	149.20	168.29	156.67	176.12	164.13	183.77
141.88	159.87	149.35	168.52	156.82	176.33	164.29	183.94
142.04	160.07	149.50	168.75	156.97	176.54	164.44	184.12
142.19	160.26	149.66	168.98	157.12	176.76	164.59	184.30
142.34	160.45	149.81	169.21	157.28	176.99	164.74	184.50
142.49	160.63	149.96	169.43	157.43	177.21	164.90	184.70
142.65	160.81	150.11	169.64	157.58	177.44	165.05	184.91
142.80	161.00	150.27	169.85	157.73	177.66	165.20	185.13

Table 3 (continued).

926B log (mbsf)	926B (rmcd)	926B log (mbsf)	926B (rmcd)	926B log (mbsf)	926B (rmcd)	926B log (mbsf)	926B (rmcd)
142.95	161.17	150.42	170.06	157.89	177.89	165.35	185.36
143.10	161.35	150.57	170.25	158.04	178.11	165.51	185.59
143.26	161.52	150.72	170.44	158.19	178.33	165.66	185.82
143.41	161.69	150.88	170.63	158.34	178.53	165.81	186.05
143.56	161.86	151.03	170.80	158.50	178.74	165.96	186.29
143.71	162.02	151.18	170.97	158.65	178.93	166.12	186.53
143.87	162.18	151.33	171.14	158.80	179.12	166.27	186.76
144.02	162.34	151.49	171.29	158.95	179.30	166.42	186.99
144.17	162.49	151.64	171.45	159.11	179.47	166.57	187.22
144.32	162.65	151.79	171.59	159.26	179.64	166.73	187.44
144.48	162.80	151.94	171.74	159.41	179.80	166.88	187.66
144.63	162.95	152.10	171.88	159.56	179.95	167.03	187.87
144.78	163.10	152.25	172.01	159.72	180.09	167.18	188.07
144.93	163.25	152.40	172.14	159.87	180.24	167.34	188.27
145.08	163.39	152.55	172.27	160.02	180.37	167.49	188.46
145.24	163.54	152.70	172.40	160.17	180.50	167.64	188.64
145.39	163.69	152.86	172.53	160.32	180.63	167.79	188.82
145.54	163.83	153.01	172.65	160.48	180.76	167.94	189.00
145.69	163.98	153.16	172.77	160.63	180.88	168.10	189.17
145.85	164.13	153.31	172.89	160.78	181.00	168.25	189.33
146.00	164.28	153.47	173.01	160.93	181.12	168.40	189.49
146.15	164.43	153.62	173.14	161.09	181.23	168.55	189.65
146.30	164.58	153.77	173.26	161.24	181.35	168.71	189.80
146.46	164.74	153.92	173.38	161.39	181.46	168.86	189.96
146.61	164.90	154.08	173.50	161.54	181.57	169.01	190.11
146.76	165.06	154.23	173.62	161.70	181.68	169.16	190.25
146.91	165.23	154.38	173.75	161.85	181.80	169.32	190.40
147.07	165.40	154.53	173.88	162.00	181.91	169.47	190.54

926B log (mbsf)	926B (rmcd)	926B log (mbsf)	926B (rmcd)	926B log (mbsf)	926B (rmcd)	926B log (mbsf)	926B (rmcd)
169.62	190.69	177.09	198.39	184.56	206.49	192.02	212.66
169.77	190.83	177.24	198.54	184.71	206.64	192.18	212.88
169.93	190.97	177.39	198.69	184.86	206.79	192.33	213.10
170.08	191.12	177.55	198.85	185.01	206.93	192.48	213.34
170.23	191.26	177.70	199.00	185.17	207.07	192.63	213.58
170.38	191.40	177.85	199.15	185.32	207.21	192.79	213.82
170.54	191.55	178.00	199.30	185.47	207.34	192.94	214.07
170.69	191.69	178.16	199.46	185.62	207.47	193.09	214.32
170.84	191.83	178.31	199.61	185.78	207.59	193.24	214.56
170.99	191.98	178.46	199.76	185.93	207.71	193.40	214.81
171.15	192.13	178.61	199.91	186.08	207.83	193.55	215.05
171.30	192.27	178.77	200.06	186.23	207.95	193.70	215.28
171.45	192.42	178.92	200.22	186.39	208.06	193.85	215.50
171.60	192.58	179.07	200.37	186.54	208.17	194.01	215.72
171.75	192.73	179.22	200.52	186.69	208.28	194.16	215.93
171.91	192.88	179.37	200.68	186.84	208.39	194.31	216.13
172.06	193.04	179.53	200.83	186.99	208.49	194.46	216.32
172.21	193.19	179.68	200.99	187.15	208.60	194.61	216.51
172.36	193.35	179.83	201.15	187.30	208.70	194.77	216.69
172.52	193.51	179.98	201.31	187.45	208.80	194.92	216.86
172.67	193.67	180.14	201.46	187.60	208.90	195.07	217.02
172.82	193.83	180.29	201.63	187.76	209.00	195.22	217.18
172.97	194.00	180.44	201.79	187.91	209.10	195.38	217.34
173.13	194.16	180.59	201.95	188.06	209.20	195.53	217.49
173.28	194.33	180.75	202.12	188.21	209.30	195.68	217.63
173.43	194.50	180.90	202.28	188.37	209.39	195.83	217.78
173.58	194.66	181.05	202.45	188.52	209.49	195.99	217.92
173.74	194.83	181.20	202.62	188.67	209.59	196.14	218.06
173.89	195.00	181.36	202.80	188.82	209.69	196.29	218.19
174.04	195.17	181.51	202.97	188.98	209.80	196.44	218.33
174.19	195.33	181.66	203.15	189.13	209.90	196.60	218.46
174.35	195.50	181.81	203.33	189.28	210.01	196.75	218.59
174.50	195.67	181.97	203.50	189.43	210.11	196.90	218.73
174.65	195.83	182.12	203.69	189.59	210.22	197.05	218.86
174.80	196.00	182.27	203.87	189.74	210.33	197.21	218.99
174.96	196.16	182.42	204.05	189.89	210.45	197.36	219.13
175.11	196.33	182.58	204.23	190.04	210.57	197.51	219.26
175.26	196.49	182.73	204.42	190.20	210.69	197.66	219.40
175.41	196.65	182.88	204.60	190.35	210.82	197.82	219.54
175.56	196.82	183.03	204.78	190.50	210.95	197.97	219.69
175.72	196.98	183.18	204.96	190.65	211.09	198.12	219.84
175.87	197.14	183.34	205.15	190.80	211.23	198.27	219.99
176.02	197.30	183.49	205.32	190.96	211.39	198.42	220.14
176.17	197.46	183.64	205.50	191.11	211.54	198.58	220.30
176.33	197.61	183.79	205.67	191.26	211.71	198.73	220.47
176.48	197.77	183.95	205.84	191.41	211.88	198.88	220.64
176.63	197.93	184.10	206.01	191.57	212.06	199.03	220.81
176.78	198.08	184.25	206.17	191.72	212.25	199.19	221.00
176.94	198.23	184.40	206.33	191.87	212.45	199.34	221.18

926B log (mbsf)	926B (rmcd)	926B log (mbsf)	926B (rmcd)	926B log (mbsf)	926B (rmcd)	926B log (mbsf)	926B (rmcd)
199.49	221.37	206.96	230.07	214.43	238.53	221.89	246.84
199.64	221.57	207.11	230.22	214.58	238.71	222.05	246.97
199.80	221.77	207.26	230.38	214.73	238.88	222.20	247.10

926B log (mbsf)	926B (rmcd)	926B log (mbsf)	926B (rmcd)	926B log (mbsf)	926B (rmcd)	926B log (mbsf)	926B (rmcd)
199.95	221.98	207.42	230.54	214.88	239.06	222.35	247.23
200.10	222.19	207.57	230.70	215.04	239.24	222.50	247.37
200.25	222.40	207.72	230.86	215.19	239.42	222.66	247.51
200.41	222.61	207.87	231.02	215.34	239.60	222.81	247.66
200.56	222.82	208.03	231.18	215.49	239.79	222.96	247.81
200.71	223.04	208.18	231.34	215.65	239.98	223.11	247.96
200.86	223.25	208.33	231.50	215.80	240.17	223.27	248.12
201.02	223.46	208.48	231.66	215.95	240.36	223.42	248.28
201.17	223.67	208.64	231.82	216.10	240.56	223.57	248.45
201.32	223.87	208.79	231.98	216.26	240.76	223.72	248.63
201.47	224.07	208.94	232.14	216.41	240.96	223.88	248.81
201.63	224.27	209.09	232.30	216.56	241.16	224.03	249.00
201.78	224.46	209.25	232.47	216.71	241.37	224.18	249.19
201.93	224.65	209.40	232.63	216.87	241.58	224.33	249.40
202.08	224.84	209.55	232.79	217.02	241.79	224.49	249.60
202.23	225.02	209.70	232.96	217.17	242.00	224.64	249.81
202.39	225.20	209.85	233.13	217.32	242.20	224.79	250.03
202.54	225.38	210.01	233.30	217.47	242.41	224.94	250.24
202.69	225.56	210.16	233.47	217.63	242.62	225.09	250.46
202.84	225.73	210.31	233.64	217.78	242.82	225.25	250.68
203.00	225.90	210.46	233.81	217.93	243.02	225.40	250.90
203.15	226.07	210.62	233.99	218.08	243.22	225.55	251.11
203.30	226.24	210.77	234.16	218.24	243.41	225.70	251.32
203.45	226.40	210.92	234.34	218.39	243.59	225.86	251.53
203.61	226.56	211.07	234.52	218.54	243.78	226.01	251.72
203.76	226.73	211.23	234.70	218.69	243.95	226.16	251.91
203.91	226.89	211.38	234.89	218.85	244.12	226.31	252.10
204.06	227.05	211.53	235.07	219.00	244.29	226.47	252.27
204.22	227.21	211.68	235.26	219.15	244.45	226.62	252.45
204.37	227.37	211.84	235.44	219.30	244.60	226.77	252.61
204.52	227.52	211.99	235.63	219.46	244.75	226.92	252.77
204.67	227.68	212.14	235.82	219.61	244.90	227.08	252.92
204.83	227.84	212.29	236.00	219.76	245.04	227.23	253.07
204.98	228.00	212.45	236.19	219.91	245.18	227.38	253.21
205.13	228.16	212.60	236.38	220.07	245.32	227.53	253.35
205.28	228.32	212.75	236.56	220.22	245.45	227.69	253.49
205.44	228.47	212.90	236.75	220.37	245.58	227.84	253.62
205.59	228.63	213.06	236.93	220.52	245.71	227.99	253.76
205.74	228.79	213.21	237.11	220.68	245.84	228.14	253.89
205.89	228.95	213.36	237.29	220.83	245.96	228.30	254.02
206.04	229.11	213.51	237.47	220.98	246.09	228.45	254.16
206.20	229.27	213.66	237.65	221.13	246.21	228.60	254.30
206.35	229.43	213.82	237.83	221.28	246.33	228.75	254.44
206.50	229.59	213.97	238.00	221.44	246.46	228.90	254.58
206.65	229.75	214.12	238.18	221.59	246.58	229.06	254.73
206.81	229.91	214.27	238.35	221.74	246.71	229.21	254.88

926B log (mbsf)	926B (rmcd)	926B log (mbsf)	926B (rmcd)	926B log (mbsf)	926B (rmcd)	926B log (mbsf)	926B (rmcd)
229.36	255.05	236.83	263.67	244.30	274.07	251.76	281.77
229.51	255.22	236.98	263.92	244.45	274.25	251.92	281.93
229.67	255.41	237.13	264.21	244.60	274.44	252.07	282.10
229.82	255.60	237.29	264.56	244.75	274.64	252.22	282.26
229.97	255.82	237.44	264.99	244.91	274.85	252.37	282.43
230.12	256.05	237.59	265.49	245.06	275.05	252.53	282.61
230.28	256.31	237.74	266.08	245.21	275.27	252.68	282.78
230.43	256.59	237.90	266.70	245.36	275.48	252.83	282.97
230.58	256.88	238.05	267.31	245.52	275.69	252.98	283.15
230.73	257.21	238.20	267.87	245.67	275.90	253.14	283.33
230.89	257.55	238.35	268.34	245.82	276.11	253.29	283.52
231.04	257.90	238.51	268.74	245.97	276.32	253.44	283.71
231.19	258.26	238.66	269.08	246.13	276.52	253.59	283.91
231.34	258.61	238.81	269.36	246.28	276.71	253.75	284.10
231.50	258.94	238.96	269.61	246.43	276.90	253.90	284.29
231.65	259.24	239.12	269.82	246.58	277.08	254.05	284.48
231.80	259.52	239.27	270.01	246.74	277.26	254.20	284.67
231.95	259.77	239.42	270.18	246.89	277.43	254.36	284.86
232.11	259.99	239.57	270.34	247.04	277.59	254.51	285.05
232.26	260.19	239.73	270.48	247.19	277.75	254.66	285.23
232.41	260.37	239.88	270.61	247.35	277.91	254.81	285.41
232.56	260.53	240.03	270.74	247.50	278.06	254.97	285.59
232.71	260.68	240.18	270.85	247.65	278.20	255.12	285.76
232.87	260.81	240.33	270.97	247.80	278.35	255.27	285.93
233.02	260.94	240.49	271.07	247.95	278.48	255.42	286.10
233.17	261.05	240.64	271.18	248.11	278.62	255.57	286.26
233.32	261.16	240.79	271.28	248.26	278.75	255.73	286.42
233.48	261.26	240.94	271.38	248.41	278.88	255.88	286.58
233.63	261.36	241.10	271.48	248.56	279.01	256.03	286.73
233.78	261.46	241.25	271.58	248.72	279.13	256.18	286.88
233.93	261.55	241.40	271.67	248.87	279.25	256.34	287.02
234.09	261.63	241.55	271.77	249.02	279.38	256.49	287.17
234.24	261.72	241.71	271.87	249.17	279.50	256.64	287.31
234.39	261.80	241.86	271.97	249.33	279.62	256.79	287.45
234.54	261.89	242.01	272.07	249.48	279.75	256.95	287.58
234.70	261.97	242.16	272.17	249.63	279.87	257.10	287.72
234.85	262.05	242.32	272.27	249.78	279.99	257.25	287.85
235.00	262.14	242.47	272.38	249.94	280.11	257.40	287.98
235.15	262.23	242.62	272.49	250.09	280.24	257.56	288.11

Table 3 (continued).

926B log (mbsf)	926B (rmcd)	926B log (mbsf)	926B (rmcd)	926B log (mbsf)	926B (rmcd)	926B log (mbsf)	926B (rmcd)
235.31	262.32	242.77	272.60	250.24	280.37	257.71	288.24
235.46	262.41	242.93	272.72	250.39	280.50	257.86	288.36
235.61	262.51	243.08	272.85	250.55	280.63	258.01	288.49
235.76	262.61	243.23	272.97	250.70	280.76	258.17	288.62
235.92	262.73	243.38	273.11	250.85	280.89	258.32	288.74
236.07	262.85	243.54	273.25	251.00	281.03	258.47	288.86
236.22	262.97	243.69	273.40	251.16	281.17	258.62	288.99
236.37	263.12	243.84	273.55	251.31	281.32	258.78	289.11
236.52	263.28	243.99	273.72	251.46	281.47	258.93	289.24
236.68	263.46	244.14	273.89	251.61	281.62	259.08	289.36

926B log (mbsf)	926B (rmcd)	926B log (mbsf)	926B (rmcd)	926B log (mbsf)	926B (rmcd)	926B log (mbsf)	926B (rmcd)
259.23	289.49	266.70	297.41	274.17	304.80		
259.38	289.61	266.85	297.54	274.32	304.92		
259.54	289.74	267.00	297.67	274.47	305.03		
259.69	289.87	267.16	297.80	274.62	305.14		
259.84	290.00	267.31	297.92	274.78	305.25		
259.99	290.13	267.46	298.04	274.93	305.35		
260.15	290.27	267.61	298.17	275.08	305.46		
260.30	290.40	267.77	298.29	275.23	305.56		
260.45	290.54	267.92	298.41	275.39	305.65		
260.60	290.68	268.07	298.53	275.54	305.75		
260.76	290.82	268.22	298.65	275.69	305.85		
260.91	290.96	268.38	298.77	275.84	305.94		
261.06	291.11	268.53	298.89	276.00	306.03		
261.21	291.26	268.68	299.02	276.15	306.12		
261.37	291.41	268.83	299.15	276.30	306.21		
261.52	291.59	269.29	299.54	276.76	306.49		
261.98	292.06	269.44	299.68				
262.13	292.22	269.60	299.82				
262.28	292.39	269.75	299.96				
262.43	292.57	269.90	300.11				
262.59	292.75	270.05	300.27				
262.74	292.93	270.21	300.43				
262.89	293.11	270.36	300.59				
263.04	293.30	270.51	300.76				
263.19	293.49	270.66	300.94				
263.35	293.68	270.81	301.12				
263.50	293.87	270.97	301.30				
263.65	294.06	271.12	301.49				
263.80	294.26	271.27	301.68				
263.96	294.45	271.42	301.88				
264.11	294.64	271.58	302.07				
264.26	294.83	271.73	302.26				
264.41	295.02	271.88	302.46				
264.57	295.20	272.03	302.65				
264.72	295.39	272.19	302.84				
264.87	295.57	272.34	303.02				
265.02	295.75	272.49	303.20				
265.18	295.92	272.64	303.37				
265.33	296.09	272.80	303.54				
265.48	296.25	272.95	303.70				
265.63	296.41	273.10	303.86				
265.79	296.57	273.25	304.01				
265.94	296.72	273.41	304.15				
266.09	296.86	273.56	304.29				
266.24	297.01	273.71	304.43				
266.40	297.15	273.86	304.56				
266.55	297.28	274.02	304.68				

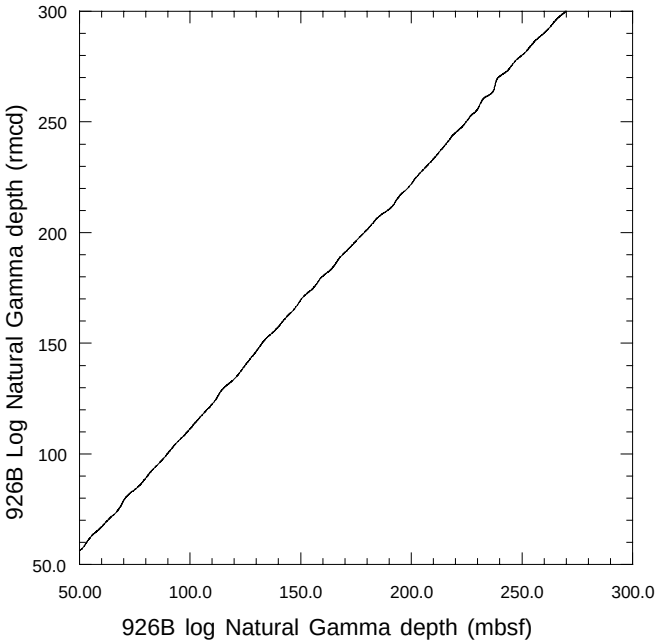

Figure 11. Mapping function relating Hole 926B log mbsf depths to Site 926 rmcd depths.

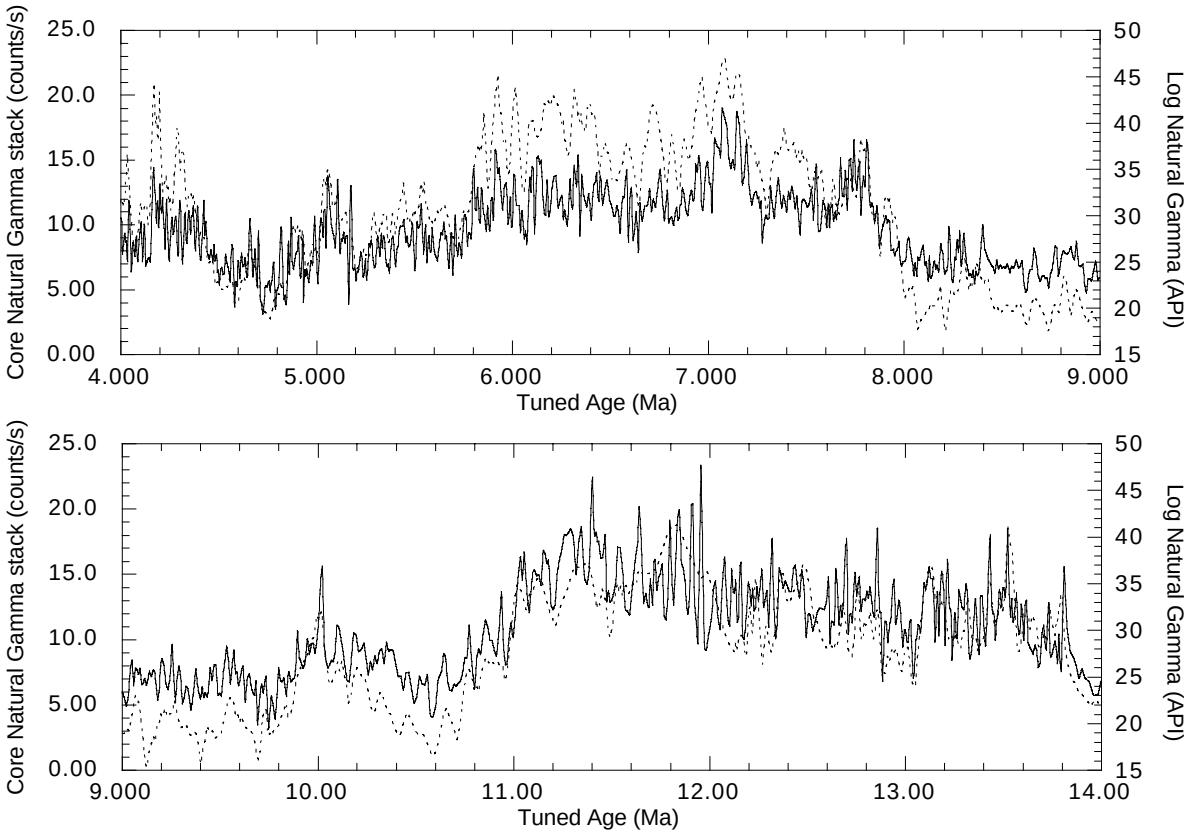

Figure 12. Site 926 NGT log natural gamma activity (dashed line) compared to Site 926 core natural gamma activity (solid line).

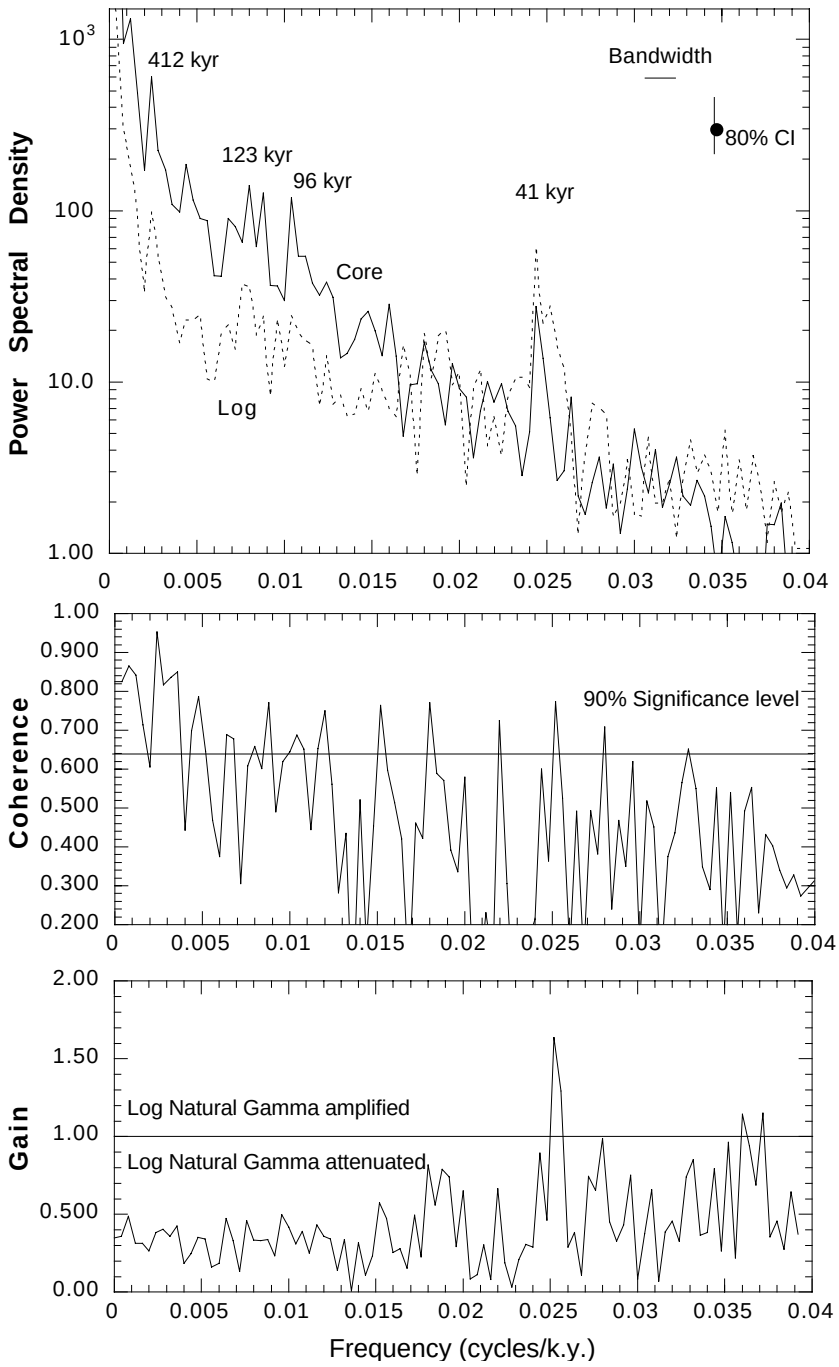

Figure 13. Power spectra of Site 926 NGT log (dashed line) and Site 926 core natural gamma activity (solid line). Spectra were calculated using 600 lags of the auto-covariance function for the time period from 1.8 to 14 Ma. Frequencies out to 25 k.y. were calculated. Coherence between the log and core data over the same interval, calculated from the cross-spectrum of the data. Horizontal line marks the significant level for nonzero coherence. Gain of the logging natural gamma variations over the core natural gamma variations. Gain values greater than 1.0 indicate log amplification relative to the core.

Previous Chapter Table of Contents Next Chapter